Energy & Environmental Science

REVIEW

Check for updates

Cite this: *Energy Environ. Sci.*, 2019, **12**, 841

Solar absorber material and system designs for photothermal water vaporization towards clean water and energy production

Minmin Gao, [a] Liangliang Zhu, [a] Connor Kangnuo Peh [a] and Ghim Wei Ho *[abc]

Received 18th April 2018,
Accepted 12th July 2018

DOI: 10.1039/c8ee01146j

rsc.li/ees

Photothermal materials with broad solar absorption and high conversion efficiency have recently attracted significant interest. They are becoming a fast-growing research focus in the area of solar-driven vaporization for clean water production. The parallel development of thermal management strategies through both material and system designs has further improved the overall efficiency of solar vaporization. Collectively, this green solar-driven water vaporization technology has regained attention as a sustainable solution for water scarcity. In this review, we will report the recent progress in solar absorber material design based on various photothermal conversion mechanisms, evaluate the prerequisites in terms of optical, thermal and wetting properties for efficient solar-driven water vaporization, classify the systems based on different photothermal evaporation configurations and discuss other correlated applications in the areas of desalination, water purification and energy generation. This article aims to provide a comprehensive review on the current development in efficient photothermal evaporation, and suggest directions to further enhance its overall efficiency through the judicious choice of materials and system designs, while synchronously capitalizing waste energy to realize concurrent clean water and energy production.

Broader context

Water and energy are scarce resources in modern society, both of which are closely linked to the economic and social development of nations. These two necessities are intertwined, with the interdependence of water and energy termed the water–energy nexus. Solar-driven vaporization using photothermal materials is a green and viable solution to address both issues, by utilizing the abundant source of solar energy. The re-emergence of solar-driven distillation has been spurred by the growing research on solar absorber materials in recent years, as this is viewed as the key to tackle solar water vaporization. Challenges which this field face include photon management, solar-to-heat conversion efficiency optimization, heat loss minimization, and control of mass transfer of water and steam. This review targets advanced photothermal nanomaterials and design architectures for energy and environmental sustainability, spanning across basic science and various engineering disciplines.

[a] *Department of Electrical and Computer Engineering, National University of Singapore, 4 Engineering Drive 3, 117583, Singapore. E-mail: elehgw@nus.edu.sg*
[b] *Engineering Science Programme, National University of Singapore, 9 Engineering Drive 1, 117575, Singapore*
[c] *Institute of Materials Research and Engineering, A*STAR (Agency for Science, Technology and Research), 2 Fusionopolis Way, 138634, Singapore*

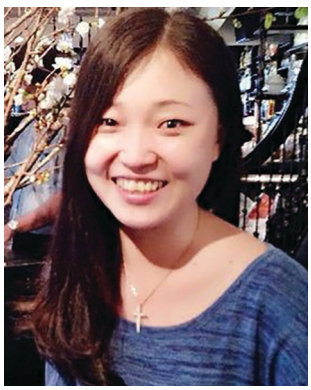

Minmin Gao

Minmin Gao received her BEng (Hons) degree in Electrical Engineering from National University of Singapore (NUS) in 2012, as well as her PhD in 2016 under the supervision of Associate Professor Dr Ghim Wei Ho. Her research interest currently focuses on nanomaterials for clean energy generation, photothermal water evaporation and photocatalytic applications.

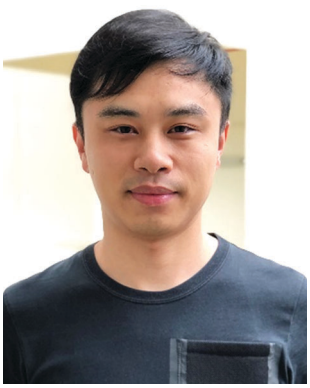

Liangliang Zhu

Liangliang Zhu received his PhD degree in Material Chemical Engineering at Nanjing University of Technology, China in 2013. He is now a research fellow at the Department of Electrical & Computer Engineering at National University of Singapore (NUS). His current research interest is preparation of photothermal materials for water evaporation and energy generation.

1. Introduction

Water and energy are basic elements pertaining to life, economic development and societal progress. In the coming decades the Earth's capacity to support humankind, especially in terms of the inextricably linked commodities of clean water and energy supplies, will be severely strained. Existing technologies that tackle water scarcity issues at the expense of aggravating energy problems or, even worse, improve access to water at the expense of the environment, cannot deliver long-term solutions. Therefore, significant efforts have been put into green technology research for clean water production.[1–7] Solar-driven water evaporation, which utilizes sunlight as a renewable energy source, is a promising approach to provide solutions for clean water scarcity with minimum environmental impact. However, the low photothermal conversion efficiency limited by both the poor solar absorption of water and heat losses due to traditional bulk water heating of the volumetric system hinders its practical applications. The recent development in nanostructured solar absorber materials has tremendously shifted attention back to the basic technology of solar-driven water evaporation due to growing concern over environmental sustainability and energy conservation. The evaporation efficiencies have been largely improved through rational designs of both nanomaterials as efficient solar absorbers and evaporation systems that utilize the concept of interfacial heating. Such an interfacial heating system with the solar absorber materials on the surface of the water confines the heat at the water–air interface which suppresses heat loss to the bulk water. These developments greatly enhance the solar evaporation efficiency and thus bring this green solar-driven water vaporization technology to a new season and motivate extensive research effort in this area.

Herein, we review the recent progress in the advancement of solar absorber material design based on (1) various photothermal conversion mechanisms, (2) photothermal conversion requirements in terms of broad absorption, thermal management and wetting properties, (3) system classifications of different solar water evaporation configurations and (4) other applications in the areas of desalination, water purification and energy generation (Fig. 1). Various nanostructured solar absorber materials, such as plasmonic metals, semiconductors and carbon-based materials with efficient photothermal conversion capabilities will be reviewed. Also, diverse approaches for enhancing the light absorption abilities of the materials, optimizing the solar-to-heat conversion efficiency, minimizing heat loss and providing effective water and/or steam transport will be discussed. Finally, a conclusion and perspective of photothermal evaporation will be presented. This review aims to offer a better understanding of photothermal conversion of various materials and to provide a guide to design solar absorber nanomaterials for deployment of solar-driven water evaporation and its potential applications in conjunction with other fields including energy and environmental areas.

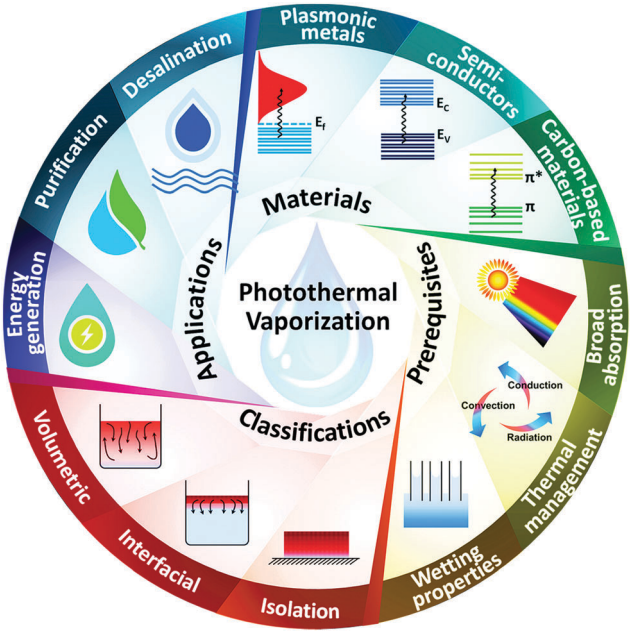

Fig. 1 Schematic drawing of the scope of this photothermal vaporization review.

Connor Kangnuo Peh

Connor Peh received his BEng (Hons) and PhD degrees from National University of Singapore in 2009 and 2016 respectively. He is currently a research fellow in NUS in A/Prof Ho Ghim Wei's group. His current research interests primarily focus on clean energy generation, photocatalytic and photoelectrochemical water splitting, and the development of materials to harness sunlight in various forms.

Ghim Wei Ho

Ghim Wei Ho received her PhD in semiconductor nanostructures at the Nanoscience Centre, University of Cambridge in 2006. She is an Associate Professor at the Department of Electrical and Computer Engineering at the National University of Singapore (NUS). She is also one of the pioneer associates of the Engineering Science Programme (ESP) at NUS. Her research thrust is focused on the development of functional nanostructured materials for energy, environmental and healthcare applications.

2. Fundamental mechanisms of photothermal conversion

Solar energy can be harnessed and converted into various kinds of energy forms including electricity, chemical (fuels), and thermal energy through photovoltaic, photochemical, and photothermal processes, respectively. Among these technologies, photothermal is a direct conversion process that possesses the highest achievable conversion efficiency. The photothermal effect is produced by photoexcitation resulting in partial or complete thermal energy (heat) production. This effect can be observed in inorganic materials, such as noble metals and semiconductors, as well as organic materials such as carbon-based materials, dyes and conjugated polymers. Adopting nanostructured materials as heat generators for harvesting solar illumination is an emerging approach to utilize solar energy for a wide range of applications, such as steam generation, domestic water heating, distillation, desalination, purification, and photothermal catalysis.[6–8] One of the advantages of the nanostructured material induced photothermal effect is its precision in heat modulation to a defined region down to the nanoscale. Moreover, nanomaterials, owing to their unique electronic and optical properties, display localized surface plasmonic resonance, quantum confinement effects and other intriguing phenomena. All these attributes, coupled with a large surface area, tunable surface properties, and controllable structures, are favourable for photothermal functions. In the design of efficient solar thermal collector materials, both the absorption of sunlight and its conversion efficiency into thermal energy contribute to the overall photothermal performance. Based on different interaction mechanisms of electromagnetic radiation with matter, we classify them into three categories, namely plasmonic localized heating of metals, non-radiative relaxation of semiconductors, and thermal vibration of molecules.

2.1. Plasmonic localized heating

In metallic materials, electromagnetic radiation absorption is mostly triggered by intraband transitions where the free conduction electrons are excited to higher energy states within the conduction band. The absorption of radiation by this mechanism is known as free carrier absorption. For metallic materials, the optical "skin depth" is a few tens of nanometres where the thermal wave fields generated by the photothermal effect are essentially at the surface plane.[9] Nanoparticles of some noble metals, such as gold and silver, exhibit brilliant colours due to the extinction of light at a wavelength caused by the localized surface plasmon resonance (LSPR) effect of the metals.[10] LSPR is a resonant photon-induced coherent oscillation of charges which occurs when the photon frequency matches the natural frequency of metal surface electrons. This LSPR effect induces three sequential phenomena, namely near-field enhancement, hot electron generation and photothermal conversion.[11,12] The plasmonic photothermal effect is a relatively recent field of research that started in 2002, mainly used for medical applications *i.e.* photothermal cancer therapy or drug delivery.[13,14] Before this, heat generation by plasmonic nanoparticles was mostly considered as a side effect.[15] The plasmon-assisted photothermal effect (Fig. 2a) occurs when metal nanoparticles are externally illuminated at their resonance wavelengths. This causes oscillation of the electron gas, exciting electrons from the occupied states to unoccupied states, forming hot electrons subsequently leading to an athermal charge distribution.[16] The decay of these hot electrons is either through radiative emission or electron–electron interactions causing carrier multiplication.[12]

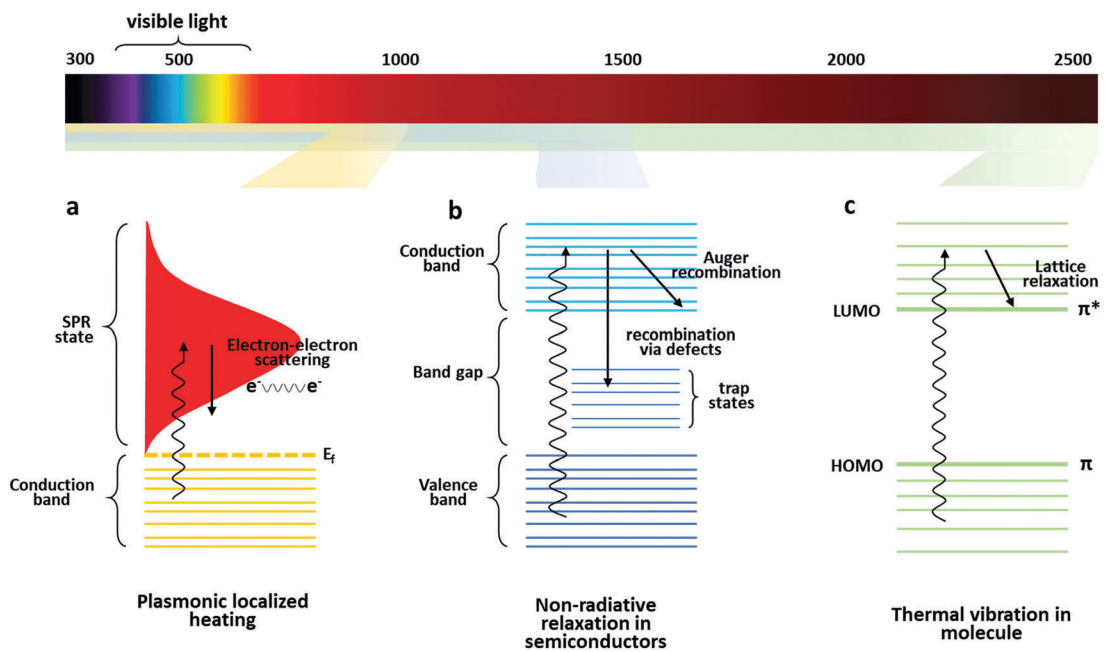

Fig. 2 Different mechanisms of the photothermal effect with the corresponding light absorption range.

The decay through electron–electron scattering redistributes the hot electron energy that leads to a rapid increase of the localized surface temperature of the metal.[17–19] This localized temperature change is followed by equilibrium cooling resulting from energy transfer from the electrons to the lattice phonons.[20] The lattice cools by phonon–phonon coupling and dissipates heat to the surrounding medium.[15] The heat generated increases the local temperature of the system.[14] The exact position and shape of the surface plasmon band depend on many factors, including the particle size,[17] the shape of the material,[18,19] the dielectric constant of the medium, and the Coulombic charge among the nanoparticles.[21] The plasmon resonance energies will determine the energy of the hot carriers generated in plasmonic materials.

2.2. Non-radiative relaxation in semiconductors

In semiconducting materials, the optical absorption shows a strong variation with the wavelength near the bandgap energy. When a semiconducting material is illuminated, electron–hole pairs are generated with an energy similar to the bandgap.[9] The excited electrons eventually return to the low-level states and release energy either through radiative relaxation in the form of photons, or non-radiative relaxation in the form of phonons (heat) by transferring the energy to impurities/defects or surface dangling bonds of the material.[22] When the energy is released in the form of phonons, it causes a local heating of the lattice which establishes a temperature distribution depending on the optical absorption and bulk/surface recombination characteristics. The photothermal effect is a result of this temperature distribution in the material due to the optically excited diffusing and recombining carriers (Fig. 2b).

2.3. Thermal vibration in molecules

Many organic materials absorb optical energy and convert it to heat through lattice vibration. Most single carbon bonds such as C–C, C–H, O–H and C–O have large energy gaps between σ and σ* that correspond to wavelengths below 350 nm in the solar spectrum. The σ to σ* transition cannot be realized under solar irradiation. On the other hand, pi (π) bonds are usually weaker than σ-bonds due to less strongly bonded electrons; these electrons can be excited from the π to the π* orbital with a lower energy input. Moreover, conjugated π bonds can also induce a red-shift in the absorption spectrum. With an increasing number of π bonds, the energy gap between the highest-occupied molecular orbital (HOMO) and the lowest unoccupied molecular orbital (LUMO) decreases. The wavelength of these bands depends on the spacing of the electronic levels. In graphene-like allotropes, the large number of conjugated π bonds facilitates the excitation of electrons by almost every wavelength of solar light irradiation, associated with various π–π* transitions, making them black coloured materials.

When a material is illuminated with light energy that matches a possible electronic transition within the molecule, an electron that absorbs the light is promoted from the ground state (HOMO) to a higher energy orbital (LUMO) as shown in Fig. 2c. The excited electrons relax by means of electron–phonon coupling, hence, the light energy absorbed is transferred from the excited electrons to vibrational modes throughout the atomic lattices, leading to a macroscopic rise in the temperature of the material.[23]

3. Criteria for efficient photothermal evaporation

Numerous studies have been done to develop and study various materials and structures for solar vaporization. Through material selection, composition tuning and surface engineering, high solar absorptance can be achieved while limiting thermal emittance and optical reflectance.[24–27] Also, systemic heat losses from conduction, convection or radiation will occur during solar to thermal conversion (Fig. 3a), and measures would have to be put in place to reduce such losses. Several critical criteria are identified that can be employed for the judicious design of solar absorber materials endowed with superior photothermal vaporization properties.

(1) Effective solar absorption – the solar absorber material is able to absorb light effectively in order to harness most of the energy from solar irradiation.

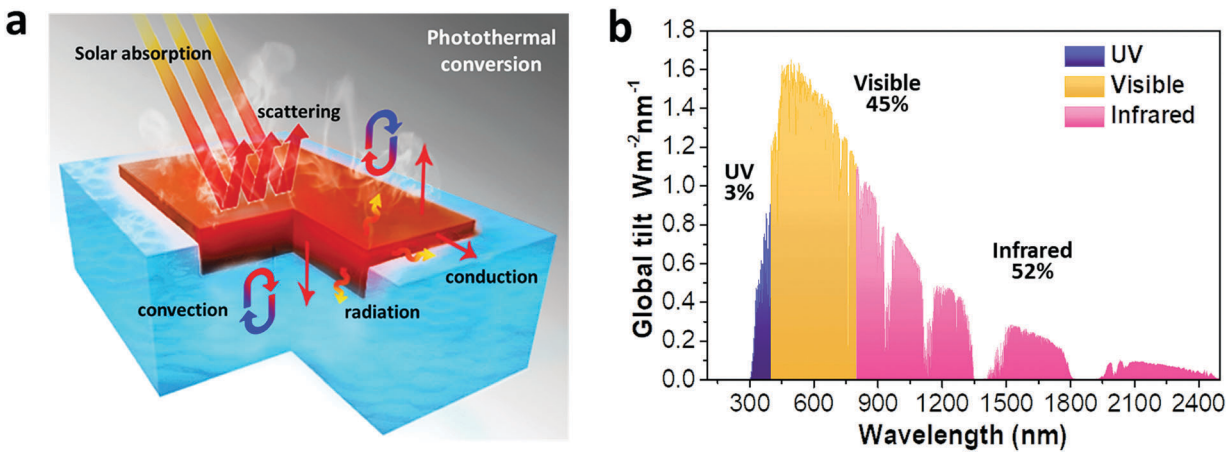

Fig. 3 (a) Schematic drawing of the photothermal conversion process for steam generation. (b) Solar spectral irradiance (AM 1.5).

(2) Efficient light to heat conversion – the light absorbed by the solar absorber material is converted to heat energy efficiently, instead of other forms of energy or being re-radiated.

(3) Appropriate thermal management – the heat generated from the absorbed light is transferred efficiently to the vaporization process, *i.e.* the thermal energy should be mostly used to overcome the latent heat of vaporization of water, while all other heat losses including heating up of bulk water and surrounding air, convection, and black body radiation losses should be minimized.

Not only do solar absorber materials need to have excellent optical and thermal properties, they should be economical and easily manufactured on a large-scale basis since the photothermal evaporation efficiency is directly proportional to the area of solar absorber materials. Additionally, they should be durable and have anti-fouling properties specifically for saltwater or polluted water vaporization applications. The following sections will discuss in detail the requirements of solar absorbers for efficient water vaporization.

3.1. Efficient solar absorption

A critical factor of how well a material converts light to heat energy is determined by the light harvesting ability of the material. This comprises two factors, the range of absorption across the solar spectrum, and the intensity of absorbance of each wavelength. Consequently, this would require the solar absorber to have a high absorbance with minimal transmittance and reflectance across the full solar spectrum range of 300 nm to 2500 nm (ASTM G-173, AM 1.5).[28] A high overall solar absorptance of the material is thus crucial to attaining a high solar to thermal efficiency.

Solar absorptance is a measure of the ability of a material to absorb solar radiation. This is determined by the ratio of the total absorbed solar radiation to the incident radiation. The total solar absorptance for a given angle of incidence θ is obtained by weighing the spectral absorptance of the material with the spectral irradiance distribution of the standard solar spectrum (AM 1.5) and integrating over the range of wavelength in which solar radiation reaches the solar absorber surface. This is then expressed as a ratio of the total solar irradiance. Eqn (3.1) describes the total solar absorptance, $\alpha(\theta)$, of a solar absorber for an incident angle of θ:

$$\alpha(\theta) = \frac{\int_{\lambda_{\min}}^{\lambda_{\max}} [1 - R(\theta, \lambda)] A(\theta, \lambda) \mathrm{d}\lambda}{\int_{\lambda_{\min}}^{\lambda_{\max}} A(\lambda) \mathrm{d}\lambda} \quad (3.1)$$

where $\lambda_{\min}$ and $\lambda_{\max}$ are 0.3 μm and 2.5 μm, respectively, and θ is the angle of incidence of light measured from the surface normal of the absorber. $A(\lambda)$ is the wavelength-dependent solar spectral irradiance. $R(\theta,\lambda)$ is the total reflectance at wavelength λ.[29]

As this review focuses on solar absorbers for vaporization purposes, using sunlight as the source of light, the material properties should aim at achieving the maximum conversion of the sunlight incident on the Earth's surface. The AM 1.5 standard lists the power distribution of solar energy incident on the Earth's surface with the following breakdown: the ultraviolet (UV) region (300–400 nm) comprising ~3% of the power, the visible range (400–700 nm) comprising ~45% of the power, and the near-infrared (NIR) region (700–2500 nm) encompassing ~52% of the power (Fig. 3b). This means that the material should have a high absorbance in the wavelengths from 300 to 2500 nm, with negligible reflectance/transmission in order to maximize the energy capture from the sun and convert it to heat energy.

3.2. Efficient light-to-heat conversion

Even though solar absorptance is a critical factor to assess solar absorber materials, the subsequent conversion of light-to-heat energy is also crucial. This would require the material to convert the energy absorbed from the sun to heat energy effectively, instead of radiative re-emission.

To compare between different materials, the conversion of light-to-heat energy is quantified as the photothermal conversion efficiency. A direct experimental method of determining the photothermal conversion efficiency is by measuring the temperature rise and consequently the heat energy generated by an incoming light source.[30–33] Typically, a light source is passed through a solution containing the solar absorber material which converts the absorbed light to heat energy resulting in an increasing overall temperature of the solution. Accounting for the heat losses by conduction and other mechanisms, the energy gained by the system (calculated by the increase in temperature and the specific heat capacity of the water) is compared to the light that is absorbed by the system to estimate the light to heat conversion efficiency.

3.3. Efficient thermal to steam generation

To produce the maximum vaporization efficiency, the heat generated by the solar absorber should be transferred entirely for the purpose of water vaporization. However, in practice, some heat will be consumed through bulk heating of water and losses to the container and surroundings by conduction, convection and radiation.

The vaporization efficiency that is often reported is the light-to-steam generation efficiency. In this case, light (often a solar simulator) is directed at a solar absorber material contained in water. The mass loss of the water is measured over time, and the energy that is used to vaporize the water is calculated. Temperatures at various parts of the system may also be measured so as to assess the increase in temperature and the uniformity of heating, by using thermocouples or infrared (IR) cameras.[3,34–37]

The efficiency η is then calculated as follows in eqn (3.2):

$$\eta = \frac{m(L_{\mathrm{v}} + Q)}{P_{\mathrm{in}}} \quad (3.2)$$

where m is the rate of mass loss of water under illumination, L_{v} is the latent heat of vaporization of water, normally taken to be 2.26 kJ g^{-1} in the region of interest, Q is the energy provided to heat the system from the initial temperature T_1 to a final temperature T_2, and P_{in} is the incident light power on the solar absorber.

4. Current development of solar absorber materials for efficient water vaporization

To date, various materials have been employed for photothermal water vaporization. Based on the different mechanisms of photothermal conversion as discussed above, different materials with efficient photothermal conversion have been developed, such as metallic materials and semiconductors, carbon-based materials, ceramic and polymers.

4.1. Metallic materials

Metallic materials are good candidates for solar receivers due to their electromagnetic radiation absorption and have been widely used as light absorbers *via* different forms, either in elementary nanoparticles or composites. Au,[8,36,38–46] Ag,[47–49] and Pd[50] have been extensively investigated and utilized in photothermal applications. Among them, Au is the most widely reported photothermal metal owing to its excellent light-to-heat converting efficiency and size/structure controllability. Various Au solar absorber structures including nanoparticles,[43] hollow spheres,[47] and nanorods[40] were reported (Fig. 4a and b). It is worth mentioning that Au does not only display the photothermal effect on its own, but also can be hybridized with other materials to improve the photothermal efficiency or to form multifunctional composites. As shown in Fig. 4c and d, composites not limited to GO–Au,[51] Au@TiO_2,[1] *etc.*[52] have already been used in the photothermally enhanced water evaporation field. Unique black gold loaded on the AAO membrane demonstrated ultra-broadband light absorption (99%), resulting in remarkably high steam generation efficiencies (Fig. 4e and f).[53,54]

Besides noble metals, low-cost Cu[55] and Al[56] have proven to possess good photothermal properties. For example, Al nanoparticles self-assembled in an AAO membrane absorb a broad solar spectrum (>96%) to achieve effective solar desalination.[56] Cauliflower-shaped hierarchical Cu nanostructures were fabricated by direct laser writing and exhibited enhanced light absorption of ~98% over a broad spectrum with a high photothermal conversion efficiency under solar illumination.[55]

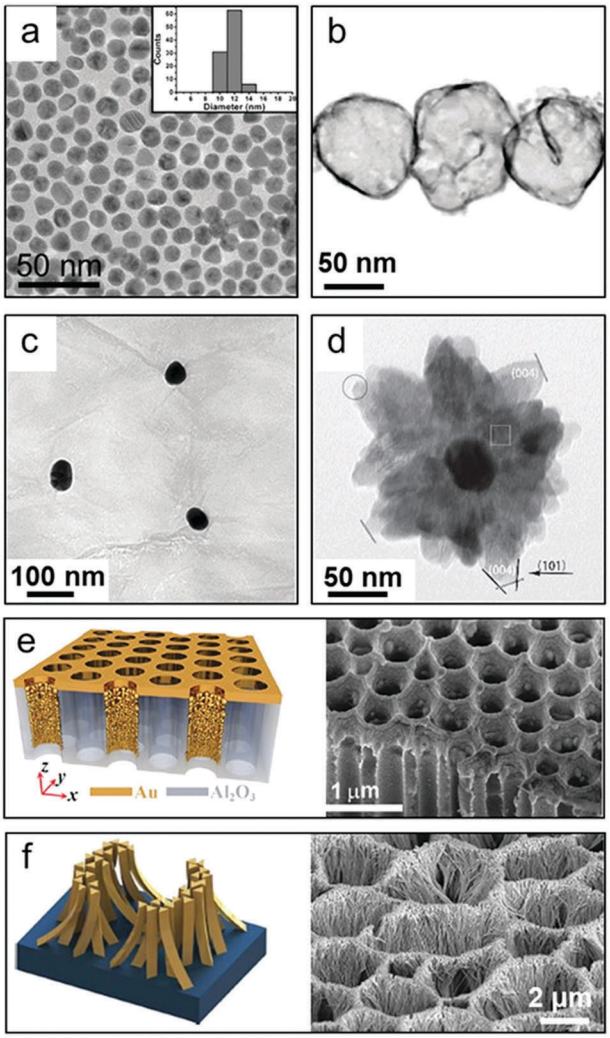

Fig. 4 TEM images of various Au nanostructures and composites: (a) particles,[43] (b) hollow spheres,[47] (c) GO–Au,[51] and (d) Au@TiO_2.[1] (e–f) Schematic illustrations and SEM images of black gold on AAO.[53,54] (a) Reprinted from ref. 43 (CC BY 4.0). (b) Reprinted with permission from ref. 47. Copyright (2016) American Chemical Society. (c) Reprinted from ref. 51, © 2016 with permission from Elsevier. (d) Reprinted from ref. 1, © 2016 with permission from Elsevier. (e) Reprinted from ref. 53 (CC BY-NC 4.0). (f) Reprinted from ref. 54 (CC BY 4.0).

4.2. Semiconductors

Semiconductor photothermal nanomaterials of metal oxides and chalcogenides have recently shown promising prospects due to their facile synthesis, low cost, invulnerability to photobleaching and photodegradation, fine-tuneable absorption spectrum and large extinction coefficients in the NIR region.[57] Copper sulphides ($Cu_{2-x}S$) have drawn significant attention for photothermal applications. Different Cu_7S_4 nanocrystals from disks to spheres have shown high photothermal evaporation performances. Hydrophobic $Cu_{12}Sb_4S_{13}$ nanoparticles with strong and full spectrum photo-absorption show an effective photothermal heating effect for vapour generation.[58] Hierarchical copper phosphate (HCuPO) has been also reported for solar evaporation.[59] Some titanium-based semiconductors such as black TiO_2,[60] black TiO_x,[61] and narrow-bandgap Ti_2O_3[62] have the ability to absorb the full spectrum of solar energy and were previously used as novel light absorbers for solar steam generation. Recyclable, non-toxic and low-cost magnetic particles including Fe_3O_4, $MnFe_2O_4$, $ZnFe_2O_4$, and $CoFe_2O_4$ have been utilized for highly efficient interfacial water evaporation.[63–65] Besides, other semiconductors *e.g.* $BiInSe_3$,[25] SnSe,[26] Al–Ti–O,[66] NiO,[67] and MoO_{3-x},[68] have also been reported and validated as effective photothermal evaporation or catalysis materials.

4.3. Carbon-based materials

Compared to metallic materials and semiconductors, carbon-based materials are cheaper, abundant, and possess excellent light absorption over a broad spectrum and high light-to-heat conversion efficiency.[69,70] Diversified carbon-based structures

from 1D to 3D have already been designed and fabricated for photothermal applications (Fig. 5). 1D CNTs on silica (Fig. 5a and b)[71] and flexible wood[72] have been used for highly efficient solar-driven interfacial water evaporation. Large surface area 2D graphene-based materials with outstanding light absorption and tunable thermal conductivity have been widely employed as the light absorber in water evaporation, purification and desalination.[2,35,73–77] Different structures of graphene-based materials including porous N-doped graphene film (Fig. 5c and d),[37] GO film, long-range vertically aligned graphene sheet membranes (Fig. 5e and f),[4] graphene and reduced graphene oxide (rGO) composite aerogels (Fig. 5g)[78,79] hierarchical graphene foam[80] and exfoliated graphite foam[81] exhibit excellent water evaporation efficiencies owing to their favourably tailored structural features. Also, other carbon-based materials such as carbon black,[3,82–85] hollow carbon beads (Fig. 5h),[86,87] carbon fabric,[88] carbon foam,[89–91] carbon sponge (Fig. 5i)[6] and coke-derived carbon[92] have been explored for water evaporation.

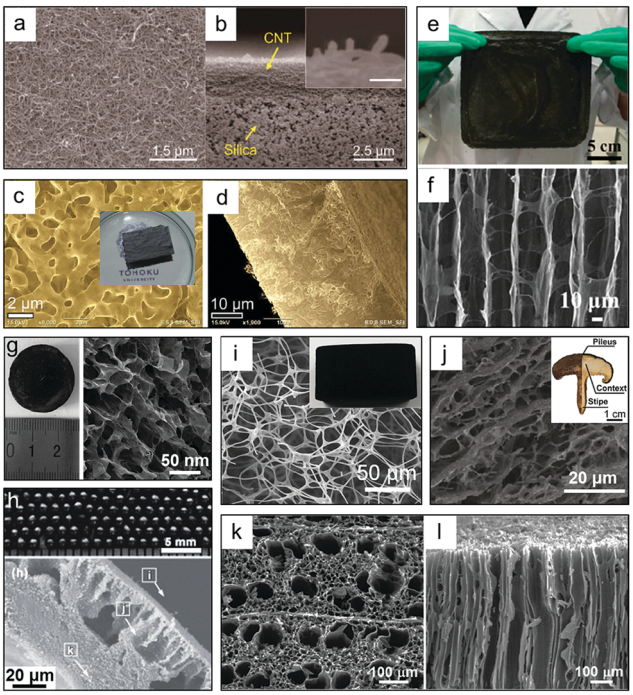

Fig. 5 SEM and digital images of various carbon-based materials. (a and b) CNTs on silica,[71] (c and d) porous N-doped graphene film,[37] (e and f) a vertically aligned graphene sheet membrane,[4] (g) a rGO composite aerogel,[78] (h) hollow carbon beads,[87] (i) carbon sponge,[6] (j) carbonized mushrooms[99] and (k and l) wood.[100] Reprinted with permission from ref. 4, 6, 37, 71, 78, 87, 99 and 100. (a and b) Reprinted with permission from ref. 71. Copyright (2016) American Chemical Society. (c and d) Reprinted with permission from ref. 37. Copyright 2015 Wiley-VCH Verlag GmbH & Co. KGaA. (e and f) Reprinted with permission from ref. 4. Copyright (2017) American Chemical Society. (g) Reprinted with permission from ref. 78. Copyright 2016 Wiley-VCH Verlag GmbH & Co. KGaA (h) reprinted with permission from ref. 87. Copyright 2016 Wiley-VCH Verlag GmbH & Co. KGaA (i) reprinted with permission from ref. 6. Copyright 2018 Wiley-VCH Verlag GmbH & Co. KGaA (j) Copyright 2017 Wiley-VCH Verlag GmbH & Co. KGaA f. 99. Copyright 2017 Wiley-VCH Verlag GmbH & Co. KGaA. (k and l) Reprinted with permission from ref. 100. Copyright (2017) American Chemical Society.

Biomaterials and natural products are environmentally friendly and sustainable carbon sources, which possess unique structures that are desirable for efficient photothermal applications. Through hybridization, carbonization or flame treatment, they can achieve outstanding light-to-heat conversion efficiency. Biofoam/rGO,[93] CNT/rGO,[94–96] CNT/wood,[72] GO/wood[97] and polydopamine (PDA)/wood[98] hybrids, carbonized mushrooms (Fig. 5j)[99] and carbonized wood (Fig. 5k and l)[100,101] have also been prepared to realize broadband absorption, photothermal conversion and heat localization.

4.4. Others

Apart from the three important types of photothermal materials, other materials such as ceramics (*e.g.* Si[102] and TiN nanoparticles),[103,104] Ti_3C_2 MXene,[105] organic polymers (polypyrrole and PPy[106,107]), and commercial products such as cermet from BlueTec Eta Plus and black cellulose fabric from Zorb®[27,108] are also used.

5. Strategies of material system design for efficient water vaporization

Tremendous attention and efforts have been devoted to creating efficient solar absorber materials for water evaporation. Various strategies include composition tuning, structure engineering and surface modification of solar absorber materials, and rational system designs in order to achieve high solar absorptance with low thermal emittance and optical reflectance, high photothermal conversion efficiency, appropriate thermal management and effective wetting properties.[7] In this section, we will discuss various strategies to enhance the solar absorption and light-to-heat conversion efficiency of various solar absorber materials, different heat management methods, and wicking framework designs for efficient solar water vaporization.

5.1. Tuning of the solar absorption range of solar absorber materials

The foremost issue of photothermal evaporation is the solar light harvesting capability of the materials. In order to achieve high solar absorptance, tailored design of the absorber materials is essential to enhance both the intensity and the range of their optical absorption. In this section, we will discuss the various strategies for optical property tuning based on the mechanism classification of photothermal materials as mentioned earlier. There are three main categories, namely plasmonic metals, semiconductors, and carbon-based materials.

5.1.1. Plasmonic metals. The absorption of plasmonic metals is governed by the LSPR effect that is strongly correlated to the shape, size, dielectric coatings or medium around the particle and the assembly state.[19,20] Therefore, the commonly used strategies for enhancing their optical properties are through structural engineering, dielectric environment modification and particle arrangement. The main barrier of using plasmonic metal particles as solar absorber materials is the limited absorption range only at one or a few LSPR wavelengths.

The position of the LSPR band can be changed by tuning the size or aspect ratio of various structures as shown in Fig. 6a(i–iv), however, the effect on broadening the absorption range is still limited.[109] On the other hand, by creating hollow structures (Fig. 6a(v–vi)) or reducing the shape symmetry (Fig. 6b(i)) one is able to extend the LSPR spectral band to a broader range.[110–112] For example, Liz-Marzán's group[113] has determined the absorption/heating efficiencies of various Au nanostructures with broadband absorption ranging from 400 to 1200 nm, using fluorescence nanothermometry in combination with double beam confocal microscopy. With the surface plasmon resonances of all these structures close to 808 nm, nanostars with sharp and long tips were found to have the highest heating efficiencies (~102%), followed by elongated nanorods (~95%), and symmetrical hollow nanoshells and nanocages (~68% and ~63%), and lastly short nanostars (~43%). Moreover, changing the surrounding dielectric will cause mainly a shift of the LSPR band and auxiliary broadening of the absorption to a certain extent (Fig. 6b(ii–iii)).[114] For instance, Lu *et al.*[115] have shown that the encapsulation of Au nanoparticles in ZIF-8 crystals causes the LSPR band of the Au nanoparticles to red-shift from 520 to 540 nm with simultaneously increased intensity. Furthermore, the coupling effect through the delicate arrangement of the plasmonic particles will induce both shifting and broadening of the absorption range as shown in Fig. 6b(iv and v).[32] This effect has been demonstrated by Zhu's group[56] through developing self-assembled close-packed aluminium nanoparticles along the sidewalls of the nanopores of an aluminium oxide membrane, which results in a strong plasmon hybridization effect. The mechanism has been examined through finite difference time domain (FDTD) calculations which show that the plasmon hybridization between the close proximity nanoparticles and the intrinsic alumina oxide layer induces a distinct redshift and widening of the aluminium-based LSP resonant modes. The experimental result reveals that the aluminium-based plasmonic absorber has broad absorption across the solar spectrum (>96%), due to the strong interference effect induced by the uniform periodic structure.

5.1.2. Semiconductors. The optical properties of a semiconductor strongly depend on the bandgap energy. One of the commonly used methods to extend the absorption range of semiconductors is through doping, such as adding impurities,

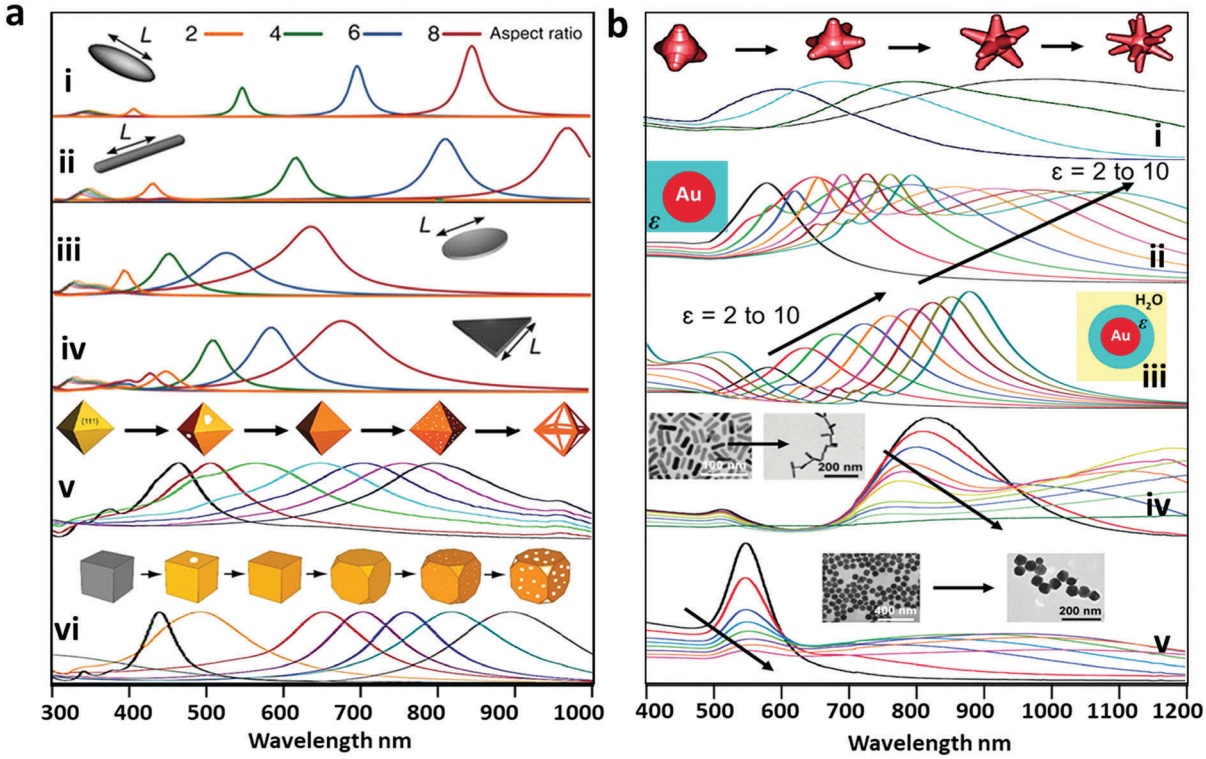

Fig. 6 The change of optical absorption of plasmonic metals with the influence of structural tuning (a-i: ellipsoid, a-ii: nanorod, a-iii: cylindrical disk and a-iv: triangular nanoprism with various aspect ratios;[109] a-v: Ag octahedra as a sacrificial template to synthesize Au nanoboxes/cages with octahedral shape;[110] a-vi: Ag nanocubes as a sacrificial template to synthesize Au nanocages;[111] b-i: Au nanostars with progressive formation of longer, sharper, and more numerous branches),[112] the dielectric environment (b-ii: an Au nanosphere (49 nm in radius) dispersed in dielectric media with varying dielectric constants; b-iii: Au–dielectric core–shell nanoparticles composed of a 49 nm radius Au core and a 36 nm thick shell with varying dielectric constants)[114] and the assembly state (b-iv: randomly arranged Au nanopolyhedrons assembled into a chain; b-v: randomly arranged Au nanorods to end-to-end assembled Au NRs).[32] (a-i–a-iv) Reprinted by permission from ref. 109 Springer Nature © 2015. (a-v) Reprinted with permission from ref. 110. Copyright (2013) American Chemical Society. (a-vi) Reprinted by permission from ref. 111 Springer Nature © 2013. (b-i) Reprinted from ref. 112. © IOP Publishing. Reproduced with permission. All rights reserved. (b-ii–b-iv) Reprinted with permission from ref. 114. Copyright (2012) American Chemical Society. (b-iv–b-v) Reprinted with permission from ref. 32 Copyright 2010 Wiley-VCH Verlag GmbH & Co. KGaA.

self-doping or introducing disorder to the nanomaterials. Doping will induce various changes to the electronic band structure of the semiconductors (Fig. 7) including (i) creating intraband energy states; (ii) narrowing of the bandgap; and (iii) impurity band formation in degenerately doped transition metal semiconductors, which broaden the absorption range of the materials to a certain extent. In this first case, the doping creates local states which function as the dominant centres for optical excitation and relaxation which extend the absorption tail of the absorption curve to longer wavelengths (Fig. 7b) compared to an intrinsic semiconductor (Fig. 7a).[116] For example, Liu's group presented oxygen-deficient MoO_{3-x} quantum dots which possess broad absorption from UV (intrinsic absorption of MoO_{3-x} due to its semiconducting nature) to both visible and NIR spectra. The broadening of light absorption has been proven to be oxygen-vacancy induced electron transitions between defect levels and other energy levels rather than LSPRs.[68] The second effect caused by doping is shifting the position of the conduction or valence band resulting in narrowing of the bandgap (Fig. 7c) and thus causing a red-shift at the edge of the absorption spectrum.[116] This method for broadening the light absorption of a solar absorber material has been demonstrated in solar steam generation applications by Wu's group. They have shown that the narrowing of the Ti_2O_3 nanoparticle bandgap results in full solar spectrum absorption (average reflectance of $<10\%$) and a high solar-thermal conversion efficiency of $\sim 92\%$.[62] Recently, the LSPR effect has been observed in degenerately doped semiconductors; these doping-induced strong LSPRs are mainly in the NIR region (Fig. 7d). Increasing the doping concentration will induce an increase in intensity as well as blue-shifts of the LSPR band.[22,117–119] For instance, Wong's group[120] synthesized Cu_7S_4 nanocrystals which exhibit strong NIR absorption originating from self-doping induced LSPR of $Cu_{2-x}S$ nanocrystals and achieve a maximum photothermal conversion efficiency of 77.1%. In addition, doping not only causes broadening of the optical absorption range but also improves the photothermal conversion efficiency due to the higher probability of non-radiative recombination in the presence of more free carriers in the semiconductor.

5.1.3. Carbon-based materials. Carbon-based materials, including carbon black, graphite, carbon nanotubes, and graphene, are well-known photothermal materials with broad light absorption that covers the whole solar spectrum. The focus of improving the solar absorption ability of carbon-based materials is not so much on the absorption range but rather increasing the intensity and minimizing surface light reflection. Creating nanostructures with pores is an effective approach to enhance the light absorption of carbon-based materials. Porous nanostructures can reduce light reflection due to the reduced effective refractive index of the materials and minimized angular dependence of the incident light. Moreover, the pores serve as optical microcavities for confining light through multiple light reflection and scattering, which greatly enhance the light–material interaction.[121] Various strategically designed porous carbon-based nanostructures have been synthesized to achieve efficient light absorption for steam generation. These porous structures can be made from 1D or 2D components, such as 1D carbon nanotube arrays on macroporous silica material that shows an average diffuse reflection of less than 2% and almost zero transmission,[71] vertically aligned 2D graphene sheets that absorb about 93% of UV, 98% of visible, and nearly 100% of NIR solar irradiation,[4] and graphene foam consisting of 2D graphene sheets forming a porous network that possesses a blackbody-like property with $\sim 97\%$ solar absorption accompanied by a multi-scattering effect.[76] Moreover, inherently 3D porous carbon structures have also been adopted for improved

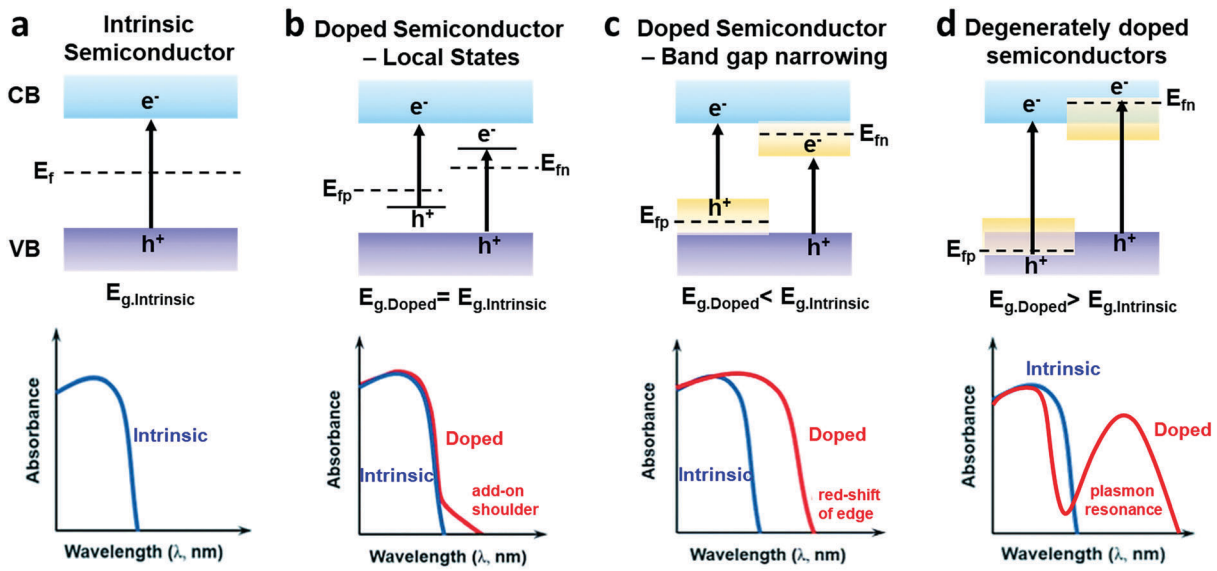

Fig. 7 Schematic for bandgap engineering of semiconductors. The band structure and optical absorption curves of (a) an intrinsic semiconductor, (b) doping-induced intraband energy states, (c) doping-induced band gap narrowing,[116] and (d) degenerate doping-induced LSPR. (a–c) Adapted from ref. 116 with permission from the Royal Society of Chemistry.

optical properties. Some of the examples are carbon sponges that exhibit extremely small optical transmittance (~0.1%) and reflectance (~3%), indicating a large optical extinction across the solar spectrum due to the increased optical path length with light scattering from nanoscale fibrils;[6] natural 3D porous carbonized wood that displays high light absorption capabilities due to the intrinsic properties of carbon-based materials and multi-scattering/reflection of light in the microchannels;[50,100,101] and carbonized mushrooms with minimized angular dependence of light absorption that enhances light absorption by 24% compared with the flat surface sample.[73]

5.1.4. Hybrid materials. Formation of hybrid materials is another approach to achieve enhanced absorption. Hybrid materials with various combinations, including bimetallic, metal–organic materials, and metal–semiconductor composites have been developed for enhanced photothermal conversion efficiency. By taking advantage of individual materials' optical properties, these hybrid materials obtain complementary and/or synergetic optical properties. For example, Zielinski *et al.*[47] revealed the synergetic effect of the geometry and material compositions of the bimetallic Ag/Au hollow structure with mesoporous shells which promotes absorption and suppress scattering in a broad spectral range. Hu's group[50] has combined the plasmonic effect of metal nanoparticles and the multi-scattering effect of microchannels in a wood matrix to achieve high solar absorption of 99% (Fig. 8a). Zhu's group[53] has also achieved light absorbance of 99% with an exceptional broad range (400 nm to 10 mm) by combining an aluminium oxide nanoporous template as an efficient light trapping medium with self-assembled Au nanoparticles of random sizes and distributions to achieve a hybridized LSPR (Fig. 8b). The synergic effect of combining various materials based on their intrinsic optical and/or structural properties contributes to improved optical properties in the absorption range and/or intensity.

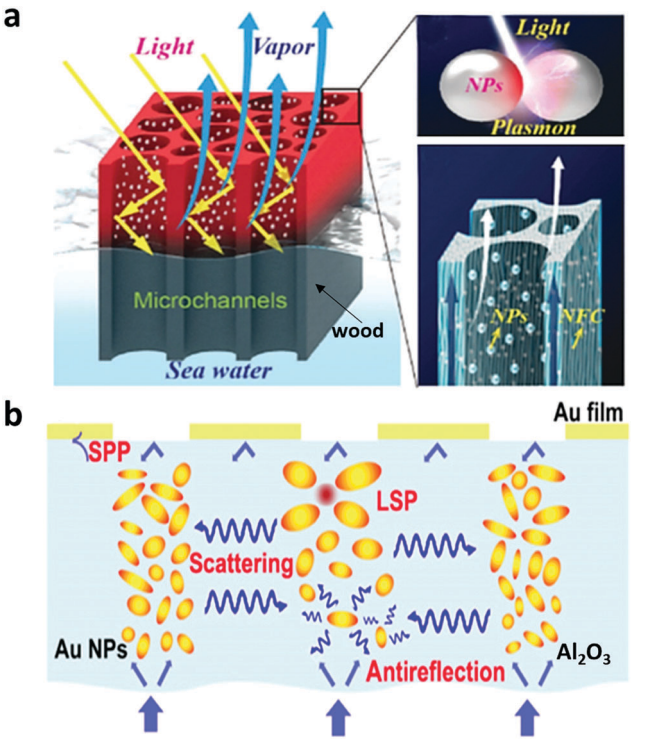

Fig. 8 (a) Design of plasmonic wood with both the plasmonic effect of metal nanoparticles and the waveguide effect of microchannels in the wood matrix.[50] (b) Schematic of a plasmonic absorber with Au nanoparticles of random sizes and distributions for the LSPR effect and nanoporous Al_2O_3 templates for efficient reflection reduction and scattering.[53] (a) Reprinted with permission from ref. 50 Copyright 2017 Wiley-VCH Verlag GmbH & Co. KGaA. (b) Reprinted from ref. 53 (CC BY-NC 4.0).

5.2. Various thermal management methods

Thermal management of solar absorber systems, both at the microscopic level as well as the macroscopic level will have a big impact on the efficient utilization of heat energy. In this case, microscopic thermal management refers to the tuning of the thermal properties of the solar absorber material, while macroscopic thermal management involves the addition of external insulation materials/components to reduce thermal loss. As heat transfer between the solar absorber and its surroundings occurs constantly, it is imperative that heat energy is directed to targeted parts of the system, *i.e.* for vaporization of water to achieve high efficiencies.

5.2.1. Microscopic thermal management. The structural design of solar absorber materials plays an important role in the thermal properties of the solar evaporation system. It has been shown that the photothermal induced temperature rise varies with the material's geometry.[7] Moreover, heat release from the solar absorber material is affected by the rate of heat generation. Meanwhile heat transfer to the surroundings is highly dependent on the surface area and thermal conductivity of the material.[13,122] Heat generation for plasmonic metal nanoparticles has been shown to have a high dependence on the size and shape of the nanoparticles (Fig. 9a).[13,123,124] Plasmonic nanostructures have a large surface area to volume ratio. The high temperatures achieved by these plasmonic particles through the photothermal conversion process, coupled with their intrinsic high thermal conductivity, would naturally result in high heat dissipation by conductance. Alternatively, by allowing contact between these plasmonic particles and the medium to be heated, the heat can be favourably channelled to the desired medium. Other nanomaterials such as foams or aerogels also possess good heat transfer properties due to the inherent large surface areas in contact with the targeted medium. Large surface areas, coupled with high thermal conductivity, enable fast heat transfer with minimal losses. Conversely, reducing the surface area or incorporating an appropriate insulating material would aid in reducing the heat transfer. Among various nanostructures, a spherical particle has been shown to be the most efficient geometry in terms of heat preservation compared with nanorods, ellipsoids, disks and rings due to its lowest surface-to-volume ratio.[14] This is useful when heat is to be confined to a specific area, to be combined with an approach that allows heat to be channelled to a specific location.[125] For material systems with broadband absorption, the heat dissipation is also through blackbody radiation.

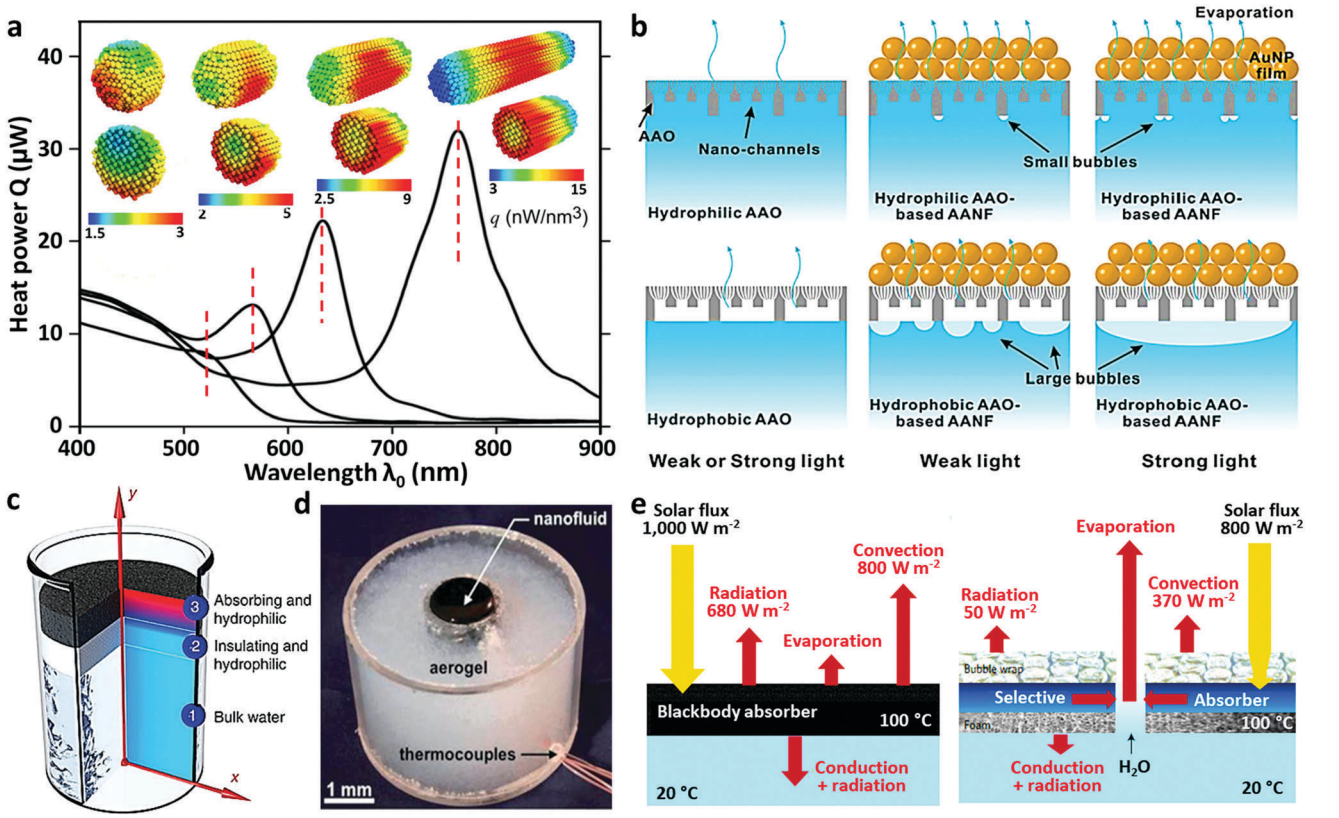

Fig. 9 (a) Calculated spectra of the heat generated in four different colloidal Au nanoparticles of the same volume with three-dimensional mapping of the heat power density computed for the four nanoparticles at their respective plasmon resonance.[124] (b) Wettability of the bottom surfaces of solar absorbing films controlling the performance localized steam generation systems: bubbles formed under the hydrophobic AAO membrane from water vaporization acted as an insulating layer limiting both heat and mass transport, compared to the hydrophilic AAO membrane which promoted efficient heat transfer and thus higher evaporation throughput.[39] (c) A solar absorber with an insulating form between the bottom surface of the solar absorber and bulk water.[35] (d) A solar absorber with external aerogel insulation to reduce conduction heat loss across the container walls.[69] (e) Energy diagram showing the incoming energy and heat losses *via* various channels in a blackbody absorber (left) and the designed selective absorber with thermal concentration (right).[27] (a) Reprinted with permission from ref. 124. Copyright 2009 AIP Publishing LLC. Reprinted with permission from ref. 124. (b) Reprinted from ref. 39 (CC BY 4.0). (c) Reprinted by permission from ref. 35 Springer Nature © 2014. (d) Reprinted from ref. 69, © 2015 with permission from Elsevier. (e) Reprinted by permission from ref. 27 Springer Nature © 2016.

However, this can be minimized by keeping the temperature difference between the solar absorber material and the surrounding medium low due to the 4th power dependence on absolute temperature according to the Stefan–Boltzmann law.

5.2.2. Macroscopic thermal management. Solar absorbers under continuous light irradiation will always be at a higher thermal state than their surroundings. In order to improve their heating efficiencies on the macroscopic level, various measures can be taken to limit the heat loss. For the application of solar water vaporization, the common approach is to limit the heat generating material to the water surface–air interface, so that the heat that is absorbed will not be transferred to the bulk water and lost through conduction or radiation.[3,36,37,63,78,86,106] In addition, a hydrophilic surface has to be in contact with the water surface in order to transfer heat efficiently to the water (Fig. 9b).[39]

It can be observed that various groups use different means to reduce conduction heat losses (Fig. 9c and d). Some have fabricated vacuum double walled glass tubes to restrict conductance losses.[34,44] Others have used aerogels, which have one of the lowest thermal conductivities of 0.03 W m^{-1} K^{-1}, as an insulating material for the container (Fig. 9d).[69] An insulating layer between the bottom surface of the solar absorber and the bulk medium such as airlaid paper[38] or insulating foam[27,35,71,93] has also been utilized to cut back heat losses. Compared to most volumetric heating with efficiencies of up to 70%,[34,51,65,69] interfacial heating systems tend to perform better with evaporation efficiencies ranging from ~60 to above 90%.[37,41,59,80,93,107]

Convection losses can be minimized by reducing the water or air flow around the system. However, re-radiation can play a big role in the system level design, especially when temperatures are elevated, since the radiation power is proportional to the fourth power of absolute temperature, and the higher the difference in temperature, the more pronounced the loss through re-radiation. Ni *et al.* did a study on the losses in a steam generation system using a blackbody absorber at 100 °C, and found that the radiative loss would amount to 680 W m^{-2} with a corresponding convection loss of 800 W m^{-2} in a surroundings temperature of 20 °C.[27] This would not be sustainable given that the incoming radiative power from the sun totals only 1000 W m^{-2}. Their group

then proposed using a selective solar absorber with a low emittance to reduce re-radiative loss significantly, to 50 W m^{-2} (Fig. 9e). They managed to achieve a solar absorber temperature of 100 °C with a corresponding efficiency of 71% (64% after accounting for evaporation in the dark). However, various other groups manage to achieve efficiencies of 70% and above even without limiting re-radiative loss. Liu *et al.* suggested that instead of losing heat to an ambient of 20 °C, the solar absorber material is covered by a film of water or heated water vapour. This means that, for their system operating at 44.2 °C, the loss to surroundings of a 41.6 °C vapour environment is only ~1.8% *via* radiation and ~ 2.6% *via* convection, leading to an efficiency of ~ 88% at 1 sun intensity. Besides, they argued that in a real enclosed solar steam system, the steam will not be released to the surroundings and the radiation would be trapped in the container.[82] As such, it is debatable whether designing the system to minimize radiative and convection losses would be significant.

Despite the differences in the various material systems, numerous groups have achieved efficiencies of 80% or more[4,73,79,100] for the different material systems. As such, it can be concluded that different material systems can be optimized such that they can perform well in the light-to-heat conversion aspect.

5.3. Design of a wicking framework

Most system designs for vaporization employ a wicking layer or channels in the material utilizing capillary action to draw water to the surface of the solar absorber.[4,73,74,82,99,100,126] With such a wicking system, the rate of evaporation would have to be matched to the rate of water being drawn up by the capillary action.

5.3.1. Intrinsic wicking. For intrinsic wicking, the solar absorber itself would inherently contain pores or channels that allow water to flow up the solar absorber *via* capillary force in order to replace the water that is lost through evaporation. These could be random pores such as those present in carbon or graphene foam,[3,37,80] graphene aerogels[78,79] or porous organic materials such as carbonized mushrooms[99] or vertically columnized channels such as wood[100] and vertically aligned graphene sheet membranes.[4]

5.3.2. External wicking. External wicking refers to materials that are added to the solar absorber, which can sometimes function as supporting structures or also insulation layers. Examples include carbon foam supports,[35] paper,[2,8,38,40] micropore tape,[54] porous anodic aluminium oxide (AAO),[39,41,53,56] porous silica,[71] nanocellulose aerogels,[93] wood,[72,97] cellulose film,[62,92,127] polyurethane[128] and aluminium foam.[81]

A special mention goes to Zhu's group which has studied the 2D wicking scheme by utilizing cellulose paper wrapped around a thermal insulator,[126] and the 1D wicking pathway by utilizing a conical shaped graphene oxide (GO) film on a supporting foam.[73]

6. Classification of various photothermal evaporation systems

Traditional concentrating solar power systems in which steam is generated from sunlight are mostly used for electricity generation. Commercially, the four leading systems used are parabolic trough collectors, solar power towers, linear Fresnel reflectors and the parabolic dish system,[129] however, conventional solar-driven steam generation systems suffer from low solar-to-steam conversion efficiency and require a high capital investment in optics and land, limiting their household and universal use. Recently, due to the development of photothermal materials, novel system designs have emerged for efficient solar-driven evaporation without the use of complicated optical concentrators. A photothermal material integrated into a water source localizes the sunlight absorption and thermal conversion as such effective heat transfer to the surrounding water media occurs. Photothermal systems can be classified into three categories (Fig. 10), according to where the solar absorber materials are placed in the liquid media.[7] The first system has the solar absorber materials dispersed in a working fluid, called the volumetric system, also known as a nanofluid (Fig. 10a and b). The second one has the solar absorbers placed on the surface of the bulk working fluid, known as the interfacial system (Fig. 10c and d). The third system has the solar absorbers separated from the bulk fluid, which is named as the isolation system (Fig. 10e and f).

6.1. Volumetric system

The volumetric system is a straightforward strategy for photothermal evaporation by direct nanostructure solar energy absorption. Unlike traditional solar-based steam production which requires heating of the bulk fluid to boiling point, the surface temperatures of the volumetric system can be lower than that of the bulk fluid, thus explicitly reducing significant heat losses to the surrounding media.[69] The steam generation mechanism for volumetric systems is still in dispute. Two possible mechanisms have been proposed to explain the vapour generation phenomenon.

6.1.1. Non-classical heat transfer (non-equilibrium heating). Halas' group from Rice University first proposed the nanoparticle–liquid non-equilibrium mechanism. Briefly, LSPR nanoparticles absorb solar energy efficiently in a liquid medium, leading to a quick increase of the nanoparticle temperature which results in the immediate surrounding water being rapidly heated up and transformed into a steam bubble (''nanobubble''). Meanwhile, the bulk fluid is still at a subcooled stage because of the poor thermal conductivity of the generated steam. Finally, the bubble buoys toward the surface and releases the steam. In this way, steam is produced without heating the entire volume of water to the boiling point, bypassing energy intensive bulk heating. Using a dilute Au nanoparticle dispersion, steam generation in an ice bath under focused sunlight *via* a Fresnel lens is realized. A thermodynamic analysis shows that 80% of the solar energy absorbed is converted into water vapour while the rest is utilized in heating the surrounding liquid.[34] Moreover, bimetallic Ag/Au hollow mesoporous plasmonic nanoshells were demonstrated by Zielinski *et al.*, yielding improved solar vapour generation. Compared to nanoparticles, each hollow nanoshell generates vapour bubbles simultaneously from the interior and the exterior when exposed to sunlight. The vapour from the interior

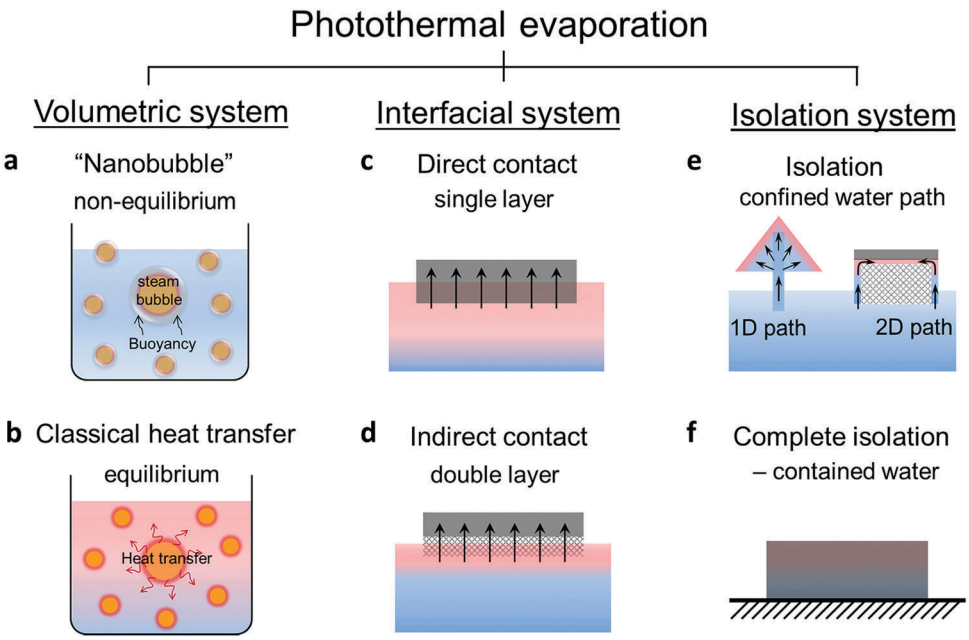

Fig. 10 Schematic drawing of various photothermal evaporation systems including (a and b) the volumetric system, (c and d) the interfacial system and (e and f) the isolation system.[7] Reproduced from ref. 7 with permission from the Royal Society of Chemistry.

combines with the bubbles formed on the outer wall after diffusing through the pores, accelerating the vapour nucleation and the overall steam generation dynamics. The hollow plasmonic nanoshells showed a conversion efficiency of 69% under solar irradiation of 11 kW m^{-2}.[47] Particularly, the "nanobubble" generation demands an intense laser source (>1000 MW m^{-2}) or highly concentrated light (>1000 suns) to overcome the energy threshold of bubble formation.[34,44,46,130] Such high illumination intensity unfavourably requires a high capital investment, including laser generator optical devices and large footprints.

6.1.2. Classical heat transfer (equilibrium heating). In this mechanism, well-dispersed solar absorbers absorb the photon energy to produce numerous micro heat sources which collectively transfer to the surrounding water to reach equilibrium with the bulk fluid. As such, the vapour generation is merely due to the rise in the bulk fluid temperature. Using three water-based nanofluids, namely graphitized carbon black, graphene, and carbon black suspensions, classical global heating for steam generation has been verified experimentally and theoretically under light concentration of 10 suns.[69] Numerical simulation and analytical modelling at device and nanoparticle scale have shown that at achievable levels of illumination intensities, it is improbable to attain temperature gradients that lead to nanobubble formation around the nanoparticle. This suggests that the mechanism of vapour generation from the nanofluids is associated with classical evaporation phenomena *i.e.* global heating of the bulk fluid.

Interestingly, other volumetric solar evaporation systems are reported to be capable of generating steam without reaching boiling point. This indicates a highly localized heating effect that is brought about by the light trapping of the solar absorber particles that simultaneously absorb and scatter light. Ho's group utilized SiO_2/Ag@TiO_2 core–shell nanoparticles for nonequilibrium steam generation below boiling point.[48] These nanocomposite particles manifest efficient steam generation through localized heating, reducing the thermal conductivity at the nanoparticle–liquid interface while functioning as nucleation sites for steam generation.

Notwithstanding, over perpetual light irradiation, bulk heating will inevitably arise which leads to steam generation through non-classical (nanobubble) and classical (global heating) mechanisms simultaneously. As such, the "nanobubble" hypothesis when combined with classical heat transfer can provide a more accurate description of the volumetric system after prolonged illumination.[45,131]

6.2. Interfacial system

Volumetric solar-driven steam generation systems including both non-equilibrium and equilibrium heating are susceptible to radiation, conduction and convection heat losses due to the bulk working liquid being inevitably heated up, resulting in a lower steam generation efficiency. The interfacial solar evaporation system is a promising strategy which can localize the solar heat and steam generation at the water–air interface using a non-submersible solar absorber. In this system, the thermal energy conversion is confined at the interface and only the water at the surface is heated up. Therefore, the temperature of the underneath bulk liquid remains low, hence minimizing heat loss and parasitic use of the converted thermal energy to heat up bulk water. Moreover, the surface temperature of the absorber is lower due to effective evaporation, thus reducing radiation and convection heat losses at the absorber surface. With this scheme, solar-to-vapour conversion efficiencies can reach higher than 90%.[4,40,53,56,62,80] Thus far, two distinct

configurations can be classified in terms of the relative location of the solar absorber to the water surface.

6.2.1. Direct contact configuration. Hydrophobic surfaces or light-weight absorbers with various architectures, *e.g.* nanoparticles,[36,59,63,64] millimeter-spheres,[86,87] films,[3,37,61,106] fiber wool,[104] monolithic aerogels and foams[6,78–81] were reported as self-floating solar absorbers. They exhibit efficient photothermal steam generation without heating the entire fluid volume. Various nanoparticles, such as films made of plasmonic Au,[36] Fe_3O_4, $MnFe_2O_4$, $ZnFe_2O_4$, $CoFe_2O_4$,[64] and carbon particles decorated with Fe_3O_4,[63] can be self-assembled into floating thin films to achieve the interfacial heating effect. The water evaporation efficiencies were significantly enhanced to about two times higher than that of the nanoparticle suspension. Similarly, millimetre sized self-floating hollow carbon spheres (HCSs) which possess an interpenetrating, open-porous carbon shell and huge external voids, permit rapid transport of molecules throughout the hollow structure.[86,87] These HCSs showed an enhanced water evaporation rate of salt water (salinity of 3.5%) by more than two times under simulated sunlight.[87]

Aside from self-floating means, films consisting of an absorber material coating on light-weight and hydrophobic scaffolds (stainless steel (SS) mesh, polypropylene (PP) mesh, gauze, or carbon fabric) were also reported.[3,61,88,107] Higgins *et al.* utilized carbon fabric (CF) for efficient solar steam generation. Due to its broadband absorbance, macroporous structure and low thermal conductivity, the CF displayed a high light-to-heat conversion efficiency of 60.2% at an incident light power density of 1 kW m^{-2}.[88] Likewise, carbon black, polypyrrole (PPy) and black TiO_x coated onto superhydrophobic gauze, SS and PP meshes were also reported to be superior light absorbers for interfacial water evaporation.

Apart from the self-floating 2D film-like solar absorbers, 3D monolithic aerogels and foam nanostructures have been reported for interfacial solar evaporation. The intrinsic porous network provides water supply paths, vapour escape channels and heat insulation that are beneficial for solar steam generation. Gao *et al.* synthesized a new hierarchical architecture utilizing vertical 1D CuO nanowires coupled with 2D graphdiyne (GDY) on 3D Cu foam as shown in Fig. 11a. In this hierarchical approach, the Cu foam serves as the supporting framework, while the CuO nanowires and GDY nanosheets are used for solar absorption and light trapping, respectively. Such a tailored structure shows excellent light absorption over the whole solar spectrum, and possesses porous networks for efficient vapour flow, demonstrating 91% photothermal efficiency under 1 kW m^{-2} illumination.[70] Other designs of similar structure, for instance, hierarchical graphene (h-G) foam with a vertical graphene nanoplate array on a 3D foam skeleton[80] and transition metal dichalcogenides (TMDCs) on macroporous nickel foam[25,26] are featured as efficient interfacial solar evaporation materials. The solar–vapour conversion efficiency of h-G foam exceeds 90% for seawater desalination. Also, traditional graphene aerogels and other carbon-based solar–thermal foam materials

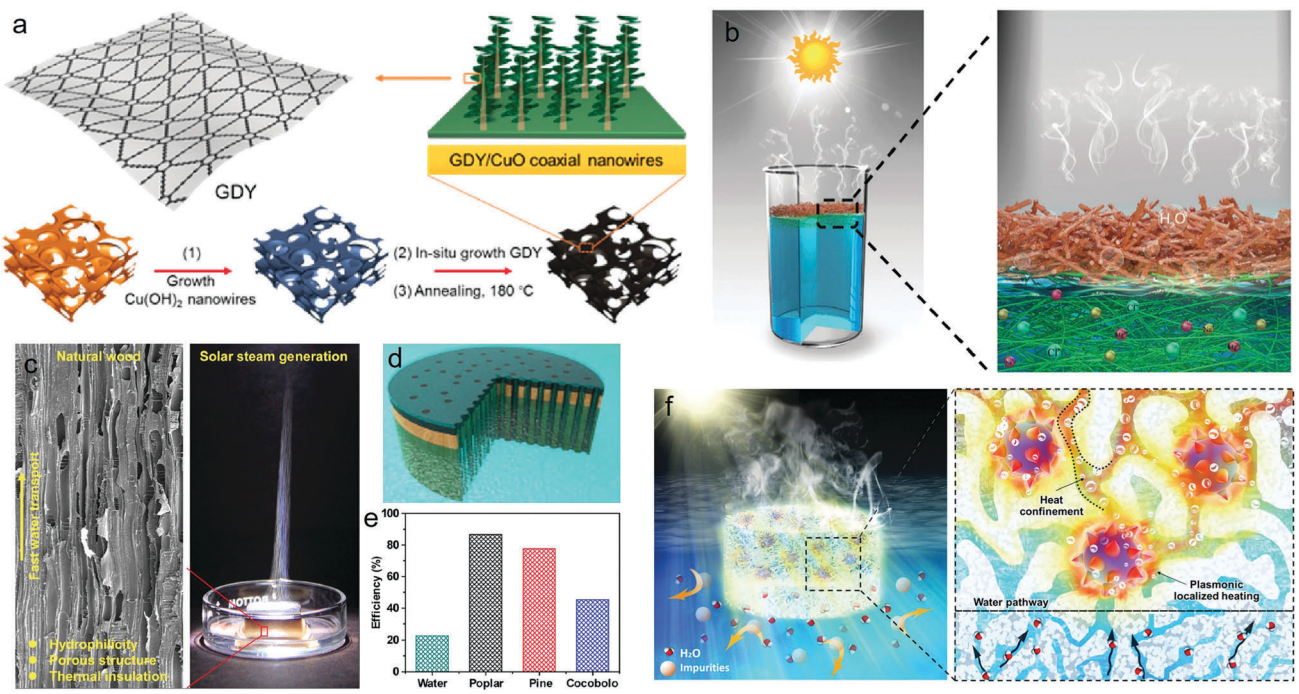

Fig. 11 (a) Schematic illustration of the GDY-based hierarchical architecture.[70] (b) Schematic of solar steam generation.[83] (c) SEM image of natural wood and digital images of the wood-based solar steam generator under light intensities of 10 suns.[101] (d) Schematic of wood-based solar steam generation.[98] (e) Comparison of the efficiency of solar steam generation for the different woods and pure water at 10 suns.[101] (f) Schematic drawing of the designed solar absorber gel for solar vaporization.[125] (a) Reprinted with permission from ref. 70. Copyright (2017) American Chemical Society (b) reprinted with permission from ref. 83 Copyright 2018 Wiley-VCH Verlag GmbH & Co. KGaA. (c and e) Reprinted from ref. 101, © 2017 with permission from Elsevier. (d) Reprinted with permission from ref. 98 Copyright 2017 Wiley-VCH Verlag GmbH & Co. KGaA.

have been widely used in the direct contact configuration.[76,78,89,91,128] Chen's group prepared a standalone 3D cross-linked honeycomb graphene foam that acts as an efficient solar thermal capture and conversion device. A high specific water production rate of ~87% was achieved under 1 sun intensity in lab conditions and >80% efficiency under outdoor ambient sunlight.[76]

6.2.2. Indirect contact configuration. Bilayered structures are generally designed for the indirect contact configuration. As such, the top layer is a solar absorber material that absorbs the solar flux without contacting the bulk water. The bottom layer aims to limit the conduction of generated heat to the underlying water body and offer a mechanically stable support for the solar absorber to prevent material dispersion into the water body. Additionally, the bottom layer requires a microporous structure with interconnected channels for efficient water supply from the bulk water to the evaporation hotspot. Airlaid paper,[2,8,38,49] AAO,[39,41,53,56] cellulose[40,58,62,92,127] and polyvinylidene fluoride (PVDF) membranes,[66,105] carbon foam,[35] biofoam,[93] leaf,[85] wood,[72,97,100,101] electrospun film,[83] and silica,[71] have been employed as the backing or lining layer due to their porous structure, low density and heat insulating properties.

Commercially available membranes or substrates with their desirable intrinsic optical and/or thermal properties for solar evaporation are conveniently adopted by researchers. For example, membrane materials with textile-like porous hydrophilic material are commonly used as thermal insulator supports.[40,58] High surface roughness can produce multi-scattering of incident solar light, leading to enhanced photon absorption. The innumerable microscale pores of paper can be leveraged for capillary water flow to the hot zone, yielding rapid replenishment of water. Their low thermal conductivity acts as a good thermal insulator to prevent the heat transfer from the solar absorber film to the bulk water. Moreover, the nanoporous AAO template with reduced refractive index and small impedance mismatch will enable low reflectance and efficient light coupling within the columnar pores, resulting in a significant light absorption enhancement. Therefore, the AAO membrane is also exploited as support for the bilayered solar evaporation scheme.[53,56]

Besides commercial membranes, a self-synthesized supporting layer with special properties has also been reported recently. Zhu's group[83] synthesized a flexible Janus absorber with a two-layer electrospun film for efficient solar desalination. The two-layer structure has opposing chemistry properties with a hydrophilic bottom layer for water wicking and a hydrophobic top layer for preventing salt accumulation on the surface (Fig. 11b). Under 1 sun illumination, the Janus absorber demonstrates efficient solar steam generation (72%) and stable water output. In addition, foam-like structures have been widely used as supporting layers due to their outstanding thermal insulation and/or wicking properties. Singamaneni's group developed a novel bilayered hybrid biofoam of rGO and bacterial nanocellulose which achieved high optical absorption, photothermal conversion, heat localization, and superior water transportation which leads to solar steam generation of 83% at 10 kW m^{-2}.[93] Another double-layer structure consisting of a carbon foam layer supporting an exfoliated graphite layer also exhibited excellent solar thermal efficiencies up to 85% at 10 kW m^{-2}, and 64% at 1 kW m^{-2}.[35]

Apart from the above-mentioned man-made bilayered structures, the transpiration of trees, relying on the unique porous structure and mass/heat transport properties, has inspired the development of wood-based interfacial evaporators. Natural wood with excellent hydrophilicity and vertically aligned microchannels for effectual water transport can be exploited as a solar absorber and support for water evaporation (Fig. 11c and d).[98,101] Inspired by the critical ecological energy–water nexus, high-efficiency solar steam generation based on natural wood was demonstrated by Hu's group. Bilayered wood-based solar steam generation devices composed of radially cut wood and a top carbonized surface were obtained through a facile heating process (Fig. 11c). The variation in multiple natural wood microstructures (poplar, pine, and cocobolo woods) results in significantly different solar steam generation performances; efficiencies of 86.7%, 76.3%, and 46.8% were calculated under 10 suns, respectively (Fig. 11e). The more porous wood showed a higher evaporation efficiency.[101] Owing to its abundance, biocompatibility, hydrophilicity, low thermal conductivity and high optical absorption, wood with a natural vessel structure makes an excellent supporting layer for solar steam generation. Many studies on hybrid wood coated solar absorber materials for interfacial solar evaporation were also reported.[72,97,100]

Another configuration for indirect contact has been developed by Ho's group[125] with an all-embracing integral design of a solar absorber gel. Unlike the bilayered system, this design integrates the thermal insulation, solar absorber and wicking materials into one 3D porous gel structure (Fig. 11f). Efficient solar absorber Au nanoflowers have been incorporated into low thermal conductivity silica-gel to establish both macroscopic insulation to prevent heat loss to bulk water, and nanoscopic heat confinement at the Au nanoflowers' proximity for sustaining elevated heat. With this design, the evaporation efficiency achieved under one sun is ~85% which is 3 times higher than pure water evaporation under the same conditions. The 3D composite solar absorber gel possesses all desirable optical, thermal and wetting properties for solar-driven vaporization in an integral scheme, which minimizes the incohesiveness, incompatibilities and instability that may likely arise between the interfaces in multi-layered photothermal structures.

6.3. Isolation system

In both direct and indirect contact configurations, heat losses between the heated up interfacial medium and bulk water are inevitable due to the large contact area. To further suppress heat conduction losses, a variety of isolating structures which separate the solar absorber from bulk water have been designed and fabricated to improve the energy conversion efficiency.[99]

6.3.1 Isolation with the water path configuration. Confined water paths are constructed to link up the solar absorber and water body for efficient water supply. Tree transpiration has inspired the design of solar evaporation systems. In nature, water is pumped from the roots of a tree and transported through

xylem vessels and lumina (channels) inside the trunks and branches and finally released to the atmosphere through the leaves to achieve efficient water supply and evaporation. An artificial transpiration device, composed of a solar absorber connected with a 1D water path, has been constructed. Hu's group designed and prepared a jellyfish-like solar steam evaporator by vertical 3D printing.[95] The integrated solar steam generator consists of vertically printed porous 1D GO pillars on the solar absorber layer and inserted into the matched porous expanded polystyrene (EPS) matrix (Fig. 12a). The capillary effect of GO pillars enables fast bottom-up water transport inside their aligned microchannels and reduces heat loss to the bulk water due to the reduced contact area between the solar absorber layer and bulk water (Fig. 12b). As a result, the solar steam device exhibited an impressive evaporation efficiency of 87.5% under one-sun illumination (Fig. 12c and d). Similar structures using rGO films equipped with one or multi-wicking fabrics/pipelines along with a foam thermal insulator were also reported to be efficient solar thermal converters.[77] Likewise, other synthetic transpiration devices with umbrella-shaped structures have been fabricated to minimize heat loss and the angular dependence of light absorption. Some of the examples are carbonized mushrooms[99] and GO hollow cones with a 1D water path made of cotton rods[73] which have displayed solar steam efficiencies over ~78% and ~85% under one sun, respectively.

A 2D water path can also realize efficient water supply in an isolated evaporation configuration by wrapping a thermal insulator with a hydrophilic material to provide a 2D capillary water pathway to the top of the solar absorber material (Fig. 10e). Some of the examples adopting this configuration are based on material systems of hydrophilic porous paper,[49,126] carbon-based absorber film[74,82] and 3D-printed carbon-based walls.[94] Liu *et al.* reported a polystyrene foam (thermal insulator) that was wrapped with carbon-coated paper which served as a 2D water path and solar absorber on the top surface.[82] Due to the excellent thermal insulation between the surface liquid and the

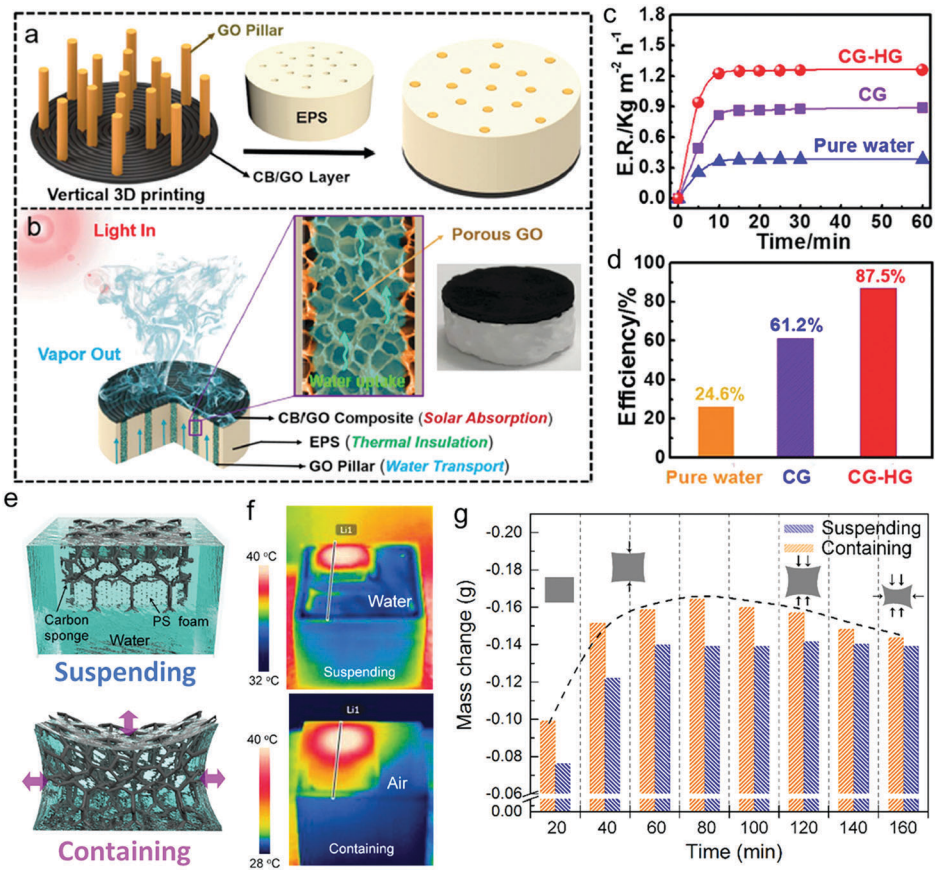

Fig. 12 (a) Structure illustration of the vertically 3D printed evaporator. The vertically 3D printed graphene oxide (GO) skeleton is inserted into the matched porous expanded polystyrene (EPS) matrix. (b) Principle illustration of the 3D printed evaporator. Water is transported inside the porous GO pillar and reaches the top surface due to the capillary effect. The carbon black/graphene oxide (CB/GO) composite layer absorbs light and converts it to thermal energy to evaporate water. The EPS matrix acts as an effective thermal insulator to suppress heat dissipation to the bulk water. The inset is the photograph showing the vertically 3D printed solar steam evaporator. (c) Evaporation rate evolutions of the pure water, CG and CG-HG (highly concentrated graphene oxide) at different time points. (d) Efficiency comparison of the pure water, CG and CG-HG under one-sun illumination.[95] (e) Schematic diagrams of CS in suspending and containing configurations. (f) The corresponding IR images of suspending and containing configurations after 30 min light irradiation. (g) The evaporation mass loss comparison of CS in contact and completely isolated from bulk water. The insets show the self-contained CS volume change with evaporation time.[6] (a–d) Reprinted from ref. 95, © 2017 with permission from Elsevier (e–g) reprinted with permission from ref. 6 Copyright 2018 Wiley-VCH Verlag GmbH & Co. KGaA.

bulk water leading to suppressed radiative and convective losses from the absorber surface to the adjacent heated vapour, a remarkable thermal efficiency of ~88% is obtained under 1 sun. 3D-printing was also employed to construct a highly-efficient solar evaporator with porous CNT/GO as a solar absorber, and a GO/nano-fibrillated cellulose (NFC) layer with a 2D GO/NFC wall as the continuous capillary water transport pathways.[94] The 3D-printed evaporator has efficient broadband solar absorption (>97%) with low thermal dissipation which results in a high conversion efficiency of 85.6% under one sun illumination.

6.3.2. Complete isolation configuration. To strictly enforce the thermal isolation effect, Ho's group has reported a novel elastic cellular sponge that self-confines and stores water without the need to be in contact with the bulk water supply.[6] The ultra-lightweight nitrogen-enriched carbon sponge can readily soak up water and conduct efficient *in situ* solar evaporation. The carbon sponge possesses favourable inbuilt structural hierarchy with mesoporous fibres that are seamlessly interconnected to form elastic macroporous open cells. The components and inbuilt structural features are beneficial to broadband light absorption and solitary heat localization. By the sponge capillary action, self-confined water is wicked and transported to perpetual hot spots so as to perform evaporation in complete isolation from the bulk water. A high efficiency of 90% was obtained, which is higher than any common suspending configuration (Fig. 12e–g).

7. Photothermal evaporation applications

With the advancement made in photothermal materials, immense attention has been brought back to traditional solar distillation which offers energy sustainability and minimum environmental impact propositions. Photothermal material based solar water evaporation has been mainly investigated for steam generation and clean water production through the distillation process as discussed earlier. However, other emerging research has integrated the solar water evaporation process with other correlated applications, including desalination, photocatalysis, wastewater treatment and electricity generation. In this section, we will explore the imminent opportunities of this green technology towards seawater desalination, water purification and energy generation.

7.1. Desalination

Desalination is one of the most important approaches to increase the fresh water supply beyond naturally existing freshwater resources.[132] Sustainable desalination driven by a renewable energy source, the sun, is an appealing method for freshwater production. As compared to membrane technology, solar-driven desalination is less susceptible to a low-quality water source and constituent concentration variations, though a highly polluted water feed may add complexity to the desalination process. However, the low efficiency due to poor solar absorption and substantial heat loss limits its practical applications. Moreover, efforts made to improve its efficiency through large optical concentrators and thermal insulation hinder its feasibility and scalability. The current progress in developing solar absorber materials for solar-driven evaporation has greatly improved the conversion efficiency, thus various systems ranging from dispersed particles and solar absorber films to bilayer structures with porous supports have been employed for solar desalination.

Volumetric systems with dispersed solar absorbing nanoparticles for solar desalination have been demonstrated by Wu's group.[65] The constructed solar desalination system is based on magnetic nanoparticle decorated reduced graphene oxide. High absorption over 95% of solar irradiation results in an evaporation efficiency of 70% under one sun. Moreover, the as-prepared nanoparticles can be easily recycled by applying an external magnetic field and their cycle stability has been tested for desalination. Another example of a volumetric system utilizes SiO_2/Ag@TiO_2 core–shell nanocomposites as an efficient solar thermal collector based on the plasmonic localized heating effect.[48] Ho's group performed real-time outdoor testing using the as-prepared SiO_2/Ag@TiO_2 nanocomposites under the sun to achieve simultaneous distillate production and photocatalytic hydrogen generation.

The interfacial system for solar desalination with direct contact has been adopted by many researchers to minimize thermal loss, and thus markedly improve the solar-to-steam conversion efficiency. Various photothermal materials, including black TiO_2 film,[60] black amorphous Al–Ti–O membranes,[66] 3D porous membranes with plasmonic nanoparticles[56] and graphene oxide coated wood[97] have been demonstrated. In order to further reduce the thermal loss to the bulk water, Zhu's group[126] employed an isolation system that contains a confined 2D water path with graphene oxide film as the solar absorber which is physically separated by a thermal insulator from the bulk water (Fig. 13a(ii)). Through this design, the efficiency under one-sun illumination reaches ~80% and the solar desalination efficiency is independent of the water quantity as shown in Fig. 13b and c. In comparison, the direct bulk water contact system only achieves an efficiency of 61% and it drops significantly to 27% as the water quantity increased to 10 cm in height (Fig. 13c). Moreover, the system is able to maintain the high efficiency without any thermal insulation, owing to its high energy transfer efficiency (78%) compared with the direct bulk water contact system (39%). Liu's group[133] has presented a bionic system with an isolation configuration which isolates the solar absorber plasmonic-active filter paper from the bulk water without an additional thermal isolation insulator (Fig. 13d). The minimization of heat loss through this design by utilizing air as the insulation material greatly increases the evaporation efficiency to ~79% under natural sunlight.

Although high-efficiency solar desalination can be achieved through the adoption of efficient solar absorber materials and low-heat-loss system designs, the deposition of salt and other solutes on the surface or in the pores of the materials during the desalination process remains a challenge for the stability

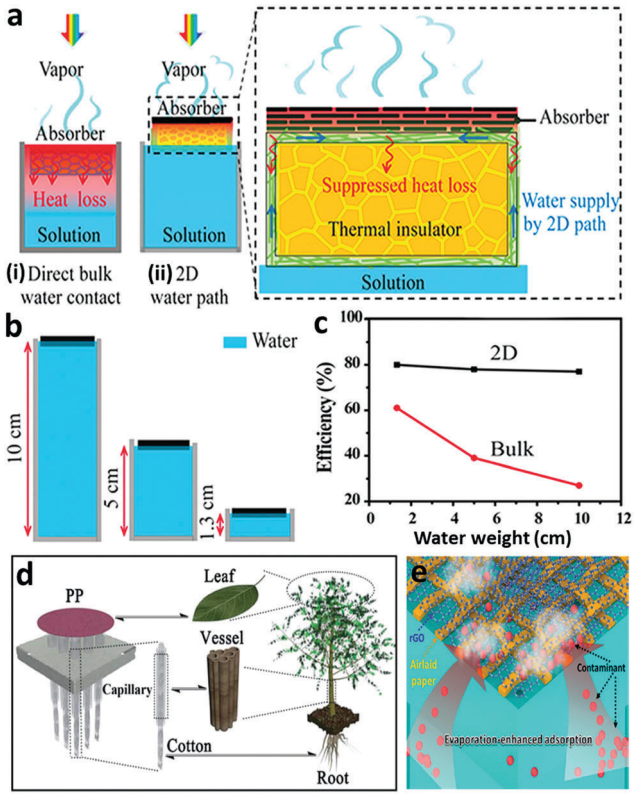

Fig. 13 (a) Schematics of (a-i) conventional solar steam generation with direct water contact and (a-ii) solar desalination devices with suppressed heat loss and 2D water supply. (b) Schematics of devices with various amount of water of height 1.3 cm, 5 cm, and 10 cm which correspond to 7 mL, 26.5 mL, and 53 mL in volume, respectively. (c) The dependence of the evaporation efficiency on the amount of water, for the 2D water path (black line) and direct bulk water contact (red line).[126] (d) Schematic diagram of the correspondence between the bionic isolation system design and a plant.[133] (e) Schematic of adsorption removal of RhB enhanced by interfacial evaporation.[2] (a–c) Reprinted from ref. 126. (d) Reproduced from ref. 133 with permission from the Royal Society of Chemistry. (e) Reprinted with permission from ref. 2. Copyright (2016) American Chemical Society.

and the recyclability of the material. Moreover, this may increase the operational costs if the materials require post-treatment or backwash after the desalination process. Therefore, more effort is needed in this area to design practical solar desalination systems with solar absorber materials of long-term usability and recyclability which have significant impacts on productivity and efficiency.

7.2. Water purification

Though elevated temperature hastens the evaporation process, it also inevitably causes unwanted residue to be evaporated and collected as impure distillate. On the other hand, utilizing solar energy to heat water to the point of evaporation *i.e.* short of boiling, can adequately evaporate water. Consequently, the water vapour condenses as pure distillate as it cools. As a result, the collected distillate will be free from most impurities and pollutants, while leaving behind unwanted residues, such as minerals, heavy metals, and microbiological organisms in the remaining water. Hence, some researchers have made efforts to couple water purification with solar evaporation in order to remove various kinds of possible contaminations in water at the same time. To date, there are mainly two different purification mechanisms that have been reported for the proposed bifunctional solar evaporation system, namely physical adsorption and photocatalytic degradation of various pollutants.

Carbon-based solar absorber materials owing to their excellent adsorption capabilities are a suitable candidate for combining water evaporation with purification functions. For example, hollow carbon spheres[87] have been investigated for fixed-bed oil adsorption and solar evaporation, while carbon fabric[88] and rGO film on air laid paper[2] have been demonstrated for effective removal of organic contaminants in industrial wastewater during solar steam generation. This purification mechanism is based on physical adsorption of the materials due to their large surface areas, desirable surface functional groups and porous structures. Moreover, Deng's group[2] has proven that solar-driven evaporation plays a dominant role in accelerating the adsorption process due to the pushing force triggered by the upward water vapour flow to the solar absorber at the water surface (Fig. 13e). However, this physical adsorption may affect the solar evaporation rate as the contaminants accumulated on the solar absorber material result in light blocking and a reduced interfacial surface area between water and the solar absorber material.

Another approach is by incorporating photocatalysts in the solar absorber material to remove organic dye contaminants through photocatalytic degradation. TiO_2 nanostructures have been integrated into both plasmonic[1] and carbon-based[2,88] solar absorber materials to demonstrate the removal of Rhodamine B (RhB) through photocatalysis. During the solar evaporation process, TiO_2 deposited on the surface of the solar absorber material absorbs UV light to generate electron–hole pairs for degradation of the pollutant RhB, while visible and NIR light will be absorbed by the solar absorber material for photothermal conversion to drive water evaporation.[2] This photocatalysis approach is often combined with physical adsorption for effective removal of the contaminants. In this case, the solar steam generation process will drive the contaminants to the porous photocatalyst-containing solar absorber material at the water surface to be adsorbed, followed by the photocatalytic degradation process that takes place at the surface of the photocatalyst. Moreover, solar evaporation further purifies the distillate, and this successive multi-step purification process is solely driven by solar energy. Nevertheless, one issue that needs to be addressed in the area of purification is the removal of volatile organic compounds (VOCs). VOCs in the water source will also evaporate during solar evaporation due to their low boiling points, and thus remain in the collected distillate. Therefore, multifunctional photothermal material designs need to be further explored with the premise of removing not only solid organic contaminants but also VOCs through adsorption, photocatalysis[134,135] or photothermal-assisted catalysis processes for water purification.[5,7]

7.3. Energy generation

Solar energy has been widely used for clean energy generation through photovoltaic, photochemical, and photothermal processes,

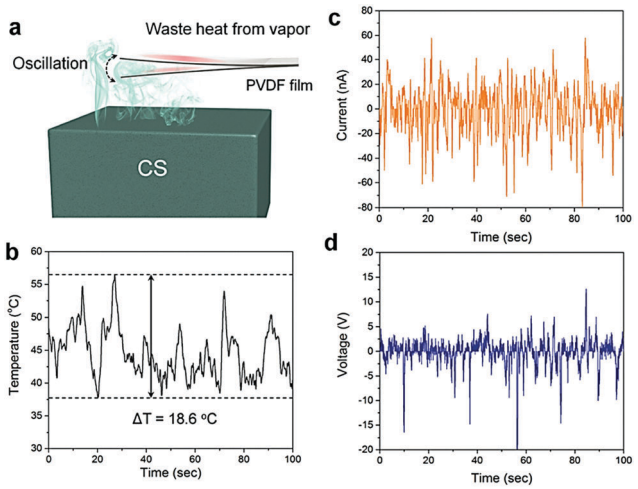

Fig. 14 (a) Schematic diagram of steam generation-induced electric potential by carbon sponge. (b) The temperature fluctuations of the PVDF film surface. The piezo-pyroelectric output currents (c) and voltages (d) of the PVDF films during the evaporation process.[6] Reprinted with permission from ref. 6. Copyright 2018 Wiley-VCH Verlag GmbH & Co. KGaA.

and combining the solar vaporization process with energy generation is a logical solution for solving water and energy scarcity issues at the same time. Recently, the integration of energy generation with the solar evaporation process for the parallel production of energy and freshwater arises. Such innovation relentlessly tackles two global challenges *i.e.* finite freshwater and fossil fuel resources. The concurrent production of various basic human needs including clean fuel and freshwater supplies powered by free sunlight further enhances the overall efficiency of photothermal conversion.

Thermal energy/heat produced during the solar vaporization process can be used either directly or indirectly for energy generation. The direct conversion of heat to electricity can be done through thermoelectric or pyroelectric devices,[136] while indirect conversion can involve photothermal-assisted photocatalysis[137,138] or piezoelectronics.[139] Ho's group[6] has scavenged the waste thermal energy generated during the evaporation process both directly and indirectly for additional electricity generation. The system is based on a complete isolation system (carbon sponge) for steam generation, while a ferroelectric fluoropolymer PVDF is used to harvest the thermomechanical responses from the generated water vapour based on the coupling of the pyroelectric and piezoelectric effects (Fig. 14a). The measured closed-circuit current and open-circuit voltage together with the temperature fluctuation are shown in Fig. 14b–d. This work provides a new opportunity for generating fresh water and clean electricity on-site or on-demand. Other work done by Ho's group[48] is the coupling of photothermal-assisted hydrogen generation and desalination using solar thermal collector nanocomposites (SiO_2/Ag@TiO_2 core–shell) to simultaneously achieve clean energy and fresh water production. The solar thermal nanocomposites address the major challenges faced in conventional catalysis and desalination systems through targeted localized heat generation at the interfacial reaction sites to reduce the thermal mass and heat losses. The all-in-one solar hydrogen and distillate production proof-of-concept prototype was used for outdoor testing to validate photothermal enhanced real-time catalysis and desalination under the real sun (Fig. 15).

In addition, other evaporation-induced energy generation systems have also been creatively designed and incorporated into solar evaporation systems. For example, Zhou's group[140] has utilized an evaporation-induced salinity difference to realize simultaneous steam and electricity generation from seawater (Fig. 16a). The hybrid system consists of carbon nanotube modified filter paper as the solar absorber material and a

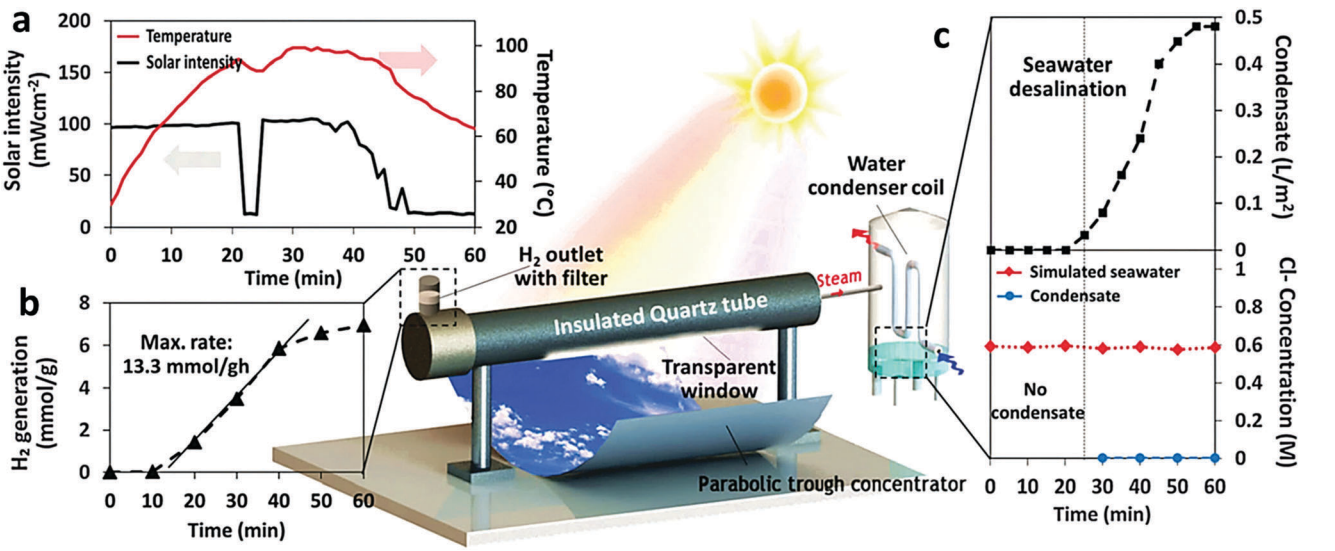

Fig. 15 Schematic of the prototype reactor with measurement of the time dependent graphs indicating (a) the solar intensity and temperature, (b) hydrogen generation, (c) the volume of the condensate (top) and the chlorine concentration (bottom).[48] Reproduced from ref. 48 with permission from the Royal Society of Chemistry.

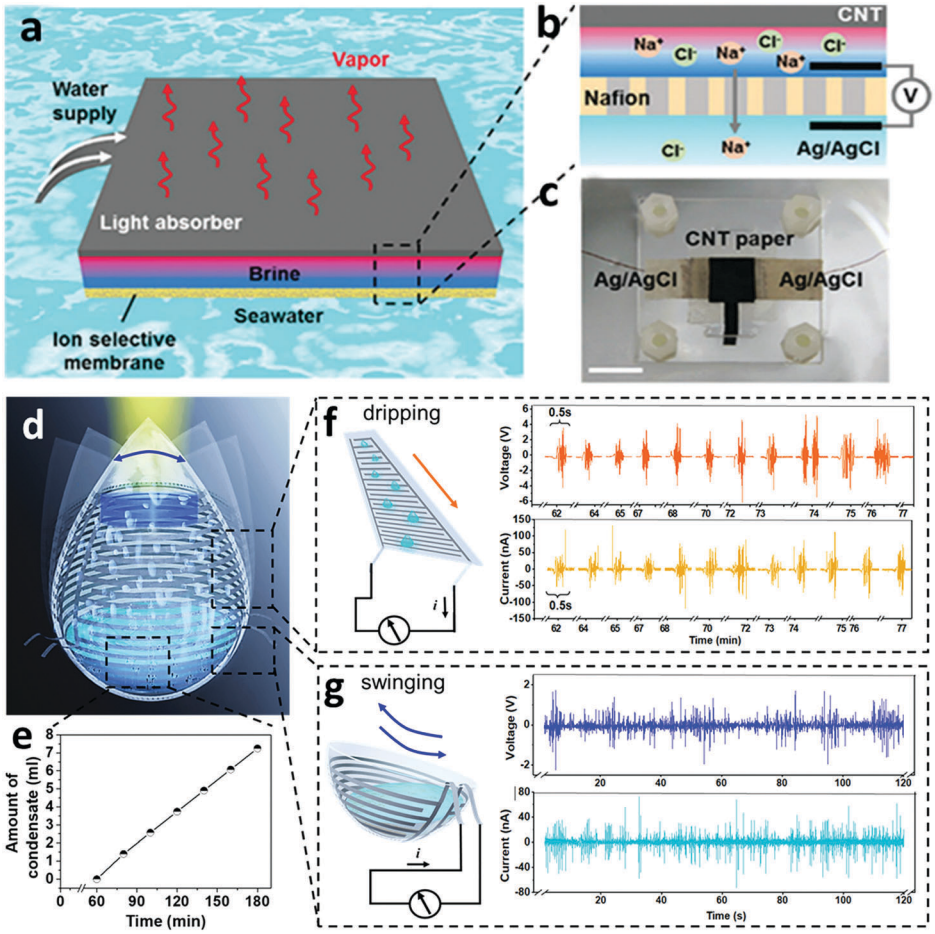

Fig. 16 (a) Schematic of the hybrid system for solar desalination and salinity power extraction. (b) Mechanism of electricity generation from the salinity difference. (c) Photograph of a hybrid device.[140] (d) Schematic diagram of the integral prototype for condensate collection and triboelectric energy generation. (e) The condensate collected under focused sunlight after the first 60 min. Schematic diagram of the triboelectric nanogenerator (TENG) for water flowing down the wall (f) and water swinging in the round bottom vessel (g) with open-circuit voltage and closed-circuit current measurements of the TENG device.[125] (a–c) Reproduced from ref. 140 with permission from the Royal Society of Chemistry.

Nafion membrane as the ion selective membrane as shown in Fig. 16b and c. The device demonstrated an efficient steam generation rate up to 75% and an electricity power of $\sim 1\ \mathrm{Wm}^{-2}$ under one sun. Their group also reported evaporation-driven water flow for electricity generation in porous carbon-based materials. This energy-harvesting technology can also be adapted to utilize solar energy to achieve hybrid water production and energy generation.[141–143] Ho's group[125] demonstrated another hybrid system that exploits the condensation process for energy generation during the solar evaporation process. An integral triboelectric nanogenerator (TENG) prototype was designed for parallel condensate collection and energy generation functions as shown in Fig. 16d and e. The enclosed system allows water vapour to condense on the wall and when the condensate flows down, it generates the triboelectric signal due to the electrification of the water and the polytetrafluoroethylene (PTFE) film adhered on the wall (Fig. 16f). The condensate is then collected at the bottom of the prototype. The round-bottom design like a roly-poly or tumbler toy is able to harvest omnidirectional mechanical energy *e.g.* wind, as such any movement/tilting raises the centre of mass, and causes it to swing in various directions. This results in triboelectricity generation due to movement of the collected condensate on the PTFE lined surface (Fig. 16g). In this case, additional energy *i.e.* triboelectricity is generated concurrently in two ways (gravitational flow and swinging of condensate) while collection of the condensate takes place during the solar evaporation process. The definitive advantages of this kind of coupling lie in increasing energy and water productivity without further stressing the environment. Moreover, multifunctional photothermal materials may promote solar energy utilization and its conversion efficiency through hybrid compatible applications.

8. Conclusion and perspective

In conclusion, we have presented a detailed review of the current development in photothermal solar absorber material and system designs for solar-driven photothermal vaporization. Various photothermal conversion mechanisms including plasmonic

localized heating, non-radiative relaxation in semiconductors and thermal vibration in carbon-based materials have been covered. Moreover, the criteria for efficient photothermal evaporation in terms of broad solar absorption, efficient thermal management and desirable wetting properties were discussed, with various strategies to improve their properties, such as material geometrical feature modifications, nanostructure designs, band-gap engineering, material constituents and solar-thermal conversion system configurations, studied for their performances. Different photothermal evaporation systems were also classified based on the relation of the absorbers to the working fluid and the designs from various research groups are presented, with the unique features highlighted. In addition, the emerging research in integrating solar-driven water evaporation with other compatible applications in both clean water production and energy generation has been reviewed.

The fast and remarkable development in photothermal materials for solar-driven evaporation in recent years greatly motivates intense research effort in this area, however, there are a few crucial challenges that need to be confronted. Firstly, although the recently reported photothermal materials are able to achieve extremely high conversion efficiencies ($>90\%$), the lack of standard experimental conditions, set-ups, efficiency calculations and performance evaluations makes it difficult to directly compare across various materials and/or systems to achieve consistent photothermal conversion efficiency and water evaporation rates analyses. Moreover, the gap between the current state-of-art and practical applications is considerable. The disparity spans across all aspects *i.e.* material long-term stability and durability in real water sources, such as seawater, natural freshwater and industrial wastewater; and the system designs and reliability for efficient condensation and water collection. Other factors that need to be considered include the influence of external factors such as wind, intermittent sunlight, the volume of water and fouling of solar absorber materials, and the removal of VOCs present in water sources which will evaporate and be collected together with the condensate. Therefore, more efforts are needed to develop robust photothermal materials with good thermal/chemical stability, recyclability and compatibility with various environments, in conjunction with the design of efficient prototypes in terms of latent heat recovery, thermal loss minimization, and a compact installation which significantly impact the overall efficiency and yield. Moreover, *in situ* and operando experimental studies, in both near and far field cases, are crucial to clearly elucidate photothermal mechanisms of various processes. Modelling of vapour flow circulation and internal heat transfer coefficients is also invaluable to better predict and access material-system performance and optimization.

In addition, solar absorber material-based photothermal evaporation as a green technology is a promising solution for clean water production due to its greatly improved efficiency compared to traditional solar distillation systems. This exciting avenue does not only bring new vitality to clean water production through photothermal evaporation from natural freshwater, seawater or polluted water, but also opens up opportunities to integrate with other correlated applications in order to achieve multifunctional devices and improve solar energy utilization. Broad potential applications ranging from direct photothermal applications such as pyroelectricity and photoactuation, to indirect photothermal-enhanced applications, such as catalysis, piezoelectricity and disinfection, enable co-generation of water, electricity or chemical fuel, from solar thermal energy.

Conflicts of interest

There are no conflicts to declare.

Acknowledgements

This research is supported by the Singapore Ministry of National Development and the National Research Foundation, Prime Minister's Office under the Land and Liveability National Innovation Challenge (L2 NIC) Research Programme (L2 NIC Award No. L2NICCFP2-2015-3).

References

1 J. Huang, Y. He, L. Wang, Y. Huang and B. Jiang, *Energy Convers. Manage.*, 2017, **132**, 452–459.
2 J. Lou, Y. Liu, Z. Wang, D. Zhao, C. Song, J. Wu, N. Dasgupta, W. Zhang, D. Zhang, P. Tao, W. Shang and T. Deng, *ACS Appl. Mater. Interfaces*, 2016, **8**, 14628–14636.
3 Y. Liu, J. Chen, D. Guo, M. Cao and L. Jiang, *ACS Appl. Mater. Interfaces*, 2015, **7**, 13645–13652.
4 P. Zhang, J. Li, L. Lv, Y. Zhao and L. Qu, *ACS Nano*, 2017, **11**, 5087–5093.
5 L. Zhu, C. F. Tan, M. Gao and G. W. Ho, *Adv. Mater.*, 2015, **27**, 7713–7719.
6 L. Zhu, M. Gao, C. K. N. Peh, X. Wang and G. W. Ho, *Adv. Energy Mater.*, 2018, **8**, 1702149.
7 L. Zhu, M. Gao, C. K. N. Peh and G. W. Ho, *Mater. Horiz.*, 2018, **5**, 323–343.
8 C. Chang, C. Yang, Y. Liu, P. Tao, C. Song, W. Shang, J. Wu and T. Deng, *ACS Appl. Mater. Interfaces*, 2016, **8**, 23412–23418.
9 P. Patel and D. Almond, *Photothermal Science and Techniques*, Chapman & Hall, London, 1st edn, 1996.
10 Z. W. Seh, S. Liu, M. Low, S.-Y. Zhang, Z. Liu, A. Mlayah and M.-Y. Han, *Adv. Mater.*, 2012, **24**, 2310–2314.
11 R. Long, Y. Li, L. Song and Y. Xiong, *Small*, 2015, **11**, 3873–3889.
12 M. L. Brongersma, N. J. Halas and P. Nordlander, *Nat. Nanotechnol.*, 2015, **10**, 25–34.
13 D. Boyer, P. Tamarat, A. Maali, B. Lounis and M. Orrit, *Science*, 2002, **297**, 1160–1163.
14 G. Baffou, R. Quidant and F. J. García de Abajo, *ACS Nano*, 2010, **4**, 709–716.
15 G. Baffou and R. Quidant, *Chem. Soc. Rev.*, 2014, **43**, 3898–3907.
16 S. Linic, U. Aslam, C. Boerigter and M. Morabito, *Nat. Mater.*, 2015, **14**, 567–576.

17 E. Ringe, M. R. Langille, K. Sohn, J. Zhang, J. Huang, C. A. Mirkin, R. P. Van Duyne and L. D. Marks, *J. Phys. Chem. Lett.*, 2012, **3**, 1479–1483.
18 S. Link, C. Burda, M. B. Mohamed, B. Nikoobakht and M. A. El-Sayed, *J. Phys. Chem. A*, 1999, **103**, 1165–1170.
19 J. A. Webb and R. Bardhan, *Nanoscale*, 2014, **6**, 2502–2530.
20 D. J. de Aberasturi, A. B. Serrano-Montes and L. M. Liz-Marzán, *Adv. Opt. Mater.*, 2015, **3**, 602–617.
21 H. Zhu, X. Chen, Z. Zheng, X. Ke, E. Jaatinen, J. Zhao, C. Guo, T. Xie and D. Wang, *Chem. Commun.*, 2009, 7524–7526, DOI: 10.1039/B917052A.
22 C. M. Hessel, V. P. Pattani, M. Rasch, M. G. Panthani, B. Koo, J. W. Tunnell and B. A. Korgel, *Nano Lett.*, 2011, **11**, 2560–2566.
23 J. R. Vélez-Cordero and J. Hernández-Cordero, *Int. J. Therm. Sci.*, 2015, **96**, 12–22.
24 V. Boriskina Svetlana, K. Tong Jonathan, W.-C. Hsu, B. Liao, Y. Huang, V. Chiloyan and G. Chen, *Nanophotonics*, 2016, **5**, 134.
25 J. D. Yao, Z. Q. Zheng and G. W. Yang, *Nanoscale*, 2017, **9**, 16396–16403.
26 J. Yao, Z. Zheng and G. Yang, *Nanoscale*, 2018, **10**, 2876–2886.
27 G. Ni, G. Li, S. V. Boriskina, H. Li, W. Yang, T. Zhang and G. Chen, *Nat. Energy*, 2016, **1**, 16126.
28 ASTM G173-03(2012), ASTM International, West Conshohocken, PA, 2012.
29 A. Amri, Z. T. Jiang, T. Pryor, C.-Y. Yin and S. Djordjevic, *Renewable Sustainable Energy Rev.*, 2014, **36**, 316–328.
30 D. K. Roper, W. Ahn and M. Hoepfner, *J. Phys. Chem. C*, 2007, **111**, 3636–3641.
31 J. R. Cole, N. A. Mirin, M. W. Knight, G. P. Goodrich and N. J. Halas, *J. Phys. Chem. C*, 2009, **113**, 12090–12094.
32 H. Chen, L. Shao, T. Ming, Z. Sun, C. Zhao, B. Yang and J. Wang, *Small*, 2010, **6**, 2272–2280.
33 K. Jiang, D. A. Smith and A. Pinchuk, *J. Phys. Chem. C*, 2013, **117**, 27073–27080.
34 O. Neumann, A. S. Urban, J. Day, S. Lal, P. Nordlander and N. J. Halas, *ACS Nano*, 2013, **7**, 42–49.
35 H. Ghasemi, G. Ni, A. M. Marconnet, J. Loomis, S. Yerci, N. Miljkovic and G. Chen, *Nat. Commun.*, 2014, **5**, 4449.
36 Z. Wang, Y. Liu, P. Tao, Q. Shen, N. Yi, F. Zhang, Q. Liu, C. Song, D. Zhang, W. Shang and T. Deng, *Small*, 2014, **10**, 3234–3239.
37 Y. Ito, Y. Tanabe, J. Han, T. Fujita, K. Tanigaki and M. Chen, *Adv. Mater.*, 2015, **27**, 4302–4307.
38 Y. Liu, S. Yu, R. Feng, A. Bernard, Y. Liu, Y. Zhang, H. Duan, W. Shang, P. Tao, C. Song and T. Deng, *Adv. Mater.*, 2015, **27**, 2768–2774.
39 S. Yu, Y. Zhang, H. Duan, Y. Liu, X. Quan, P. Tao, W. Shang, J. Wu, C. Song and T. Deng, *Sci. Rep.*, 2015, **5**, 13600.
40 C. Liu, J. Huang, C.-E. Hsiung, Y. Tian, J. Wang, Y. Han and A. Fratalocchi, *Adv. Sustainable Syst.*, 2017, **1**, 1600013.
41 L. Zhou, S. Zhuang, C. He, Y. Tan, Z. Wang and J. Zhu, *Nano Energy*, 2017, **32**, 195–200.
42 X. Chen, A. Munjiza, K. Zhang and D. Wen, *J. Phys. Chem. C*, 2014, **118**, 1285–1293.
43 D. Zhao, H. Duan, S. Yu, Y. Zhang, J. He, X. Quan, P. Tao, W. Shang, J. Wu, C. Song and T. Deng, *Sci. Rep.*, 2015, **5**, 17276.
44 H. Jin, G. Lin, L. Bai, A. Zeiny and D. Wen, *Nano Energy*, 2016, **28**, 397–406.
45 N. J. Hogan, A. S. Urban, C. Ayala-Orozco, A. Pimpinelli, P. Nordlander and N. J. Halas, *Nano Lett.*, 2014, **14**, 4640–4645.
46 Z. Fang, Y.-R. Zhen, O. Neumann, A. Polman, F. J. García de Abajo, P. Nordlander and N. J. Halas, *Nano Lett.*, 2013, **13**, 1736–1742.
47 M. S. Zielinski, J.-W. Choi, T. La Grange, M. Modestino, S. M. H. Hashemi, Y. Pu, S. Birkhold, J. A. Hubbell and D. Psaltis, *Nano Lett.*, 2016, **16**, 2159–2167.
48 M. Gao, P. K. N. Connor and G. W. Ho, *Energy Environ. Sci.*, 2016, **9**, 3151–3160.
49 J. Fang, Q. Liu, W. Zhang, J. Gu, Y. Su, H. Su, C. Guo and D. Zhang, *J. Mater. Chem. A*, 2017, **5**, 17817–17821.
50 M. Zhu, Y. Li, F. Chen, X. Zhu, J. Dai, Y. Li, Z. Yang, X. Yan, J. Song, Y. Wang, E. Hitz, W. Luo, M. Lu, B. Yang and L. Hu, *Adv. Energy Mater.*, 2018, **8**, 1701028.
51 Y. Fu, T. Mei, G. Wang, A. Guo, G. Dai, S. Wang, J. Wang, J. Li and X. Wang, *Appl. Therm. Eng.*, 2017, **114**, 961–968.
52 O. Neumann, A. D. Neumann, E. Silva, C. Ayala-Orozco, S. Tian, P. Nordlander and N. J. Halas, *Nano Lett.*, 2015, **15**, 7880–7885.
53 L. Zhou, Y. Tan, D. Ji, B. Zhu, P. Zhang, J. Xu, Q. Gan, Z. Yu and J. Zhu, *Sci. Adv.*, 2016, **2**, e1501227.
54 K. Bae, G. Kang, S. K. Cho, W. Park, K. Kim and W. J. Padilla, *Nat. Commun.*, 2015, **6**, 10103.
55 P. Fan, H. Wu, M. Zhong, H. Zhang, B. Bai and G. Jin, *Nanoscale*, 2016, **8**, 14617–14624.
56 L. Zhou, Y. Tan, J. Wang, W. Xu, Y. Yuan, W. Cai, S. Zhu and J. Zhu, *Nat. Photonics*, 2016, **10**, 393–398.
57 X. Huang, W. Zhang, G. Guan, G. Song, R. Zou and J. Hu, *Acc. Chem. Res.*, 2017, **50**, 2529–2538.
58 C. Song, T. Li, W. Guo, Y. Gao, C. Yang, Q. Zhang, D. An, W. Huang, M. Yan and C. Guo, *New J. Chem.*, 2018, **42**, 3175–3179.
59 Z. Hua, B. Li, L. Li, X. Yin, K. Chen and W. Wang, *J. Phys. Chem. C*, 2017, **121**, 60–69.
60 G. Zhu, J. Xu, W. Zhao and F. Huang, *ACS Appl. Mater. Interfaces*, 2016, **8**, 31716–31721.
61 M. Ye, J. Jia, Z. Wu, C. Qian, R. Chen, P. G. O'Brien, W. Sun, Y. Dong and G. A. Ozin, *Adv. Energy Mater.*, 2017, **7**, 1601811.
62 J. Wang, Y. Li, L. Deng, N. Wei, Y. Weng, S. Dong, D. Qi, J. Qiu, X. Chen and T. Wu, *Adv. Mater.*, 2017, **29**, 1603730.
63 Y. Zeng, J. Yao, B. A. Horri, K. Wang, Y. Wu, D. Li and H. Wang, *Energy Environ. Sci.*, 2011, **4**, 4074–4078.
64 R. Chen, Z. Wu, T. Zhang, T. Yu and M. Ye, *RSC Adv.*, 2017, **7**, 19849–19855.
65 X. Wang, G. Ou, N. Wang and H. Wu, *ACS Appl. Mater. Interfaces*, 2016, **8**, 9194–9199.

66 L. Yi, S. Ci, S. Luo, P. Shao, Y. Hou and Z. Wen, *Nano Energy*, 2017, **41**, 600–608.
67 H. Liu, X. Zhang, Z. Hong, Z. Pu, Q. Yao, J. Shi, G. Yang, B. Mi, B. Yang, X. Liu, H. Jiang and X. Hu, *Nano Energy*, 2017, **42**, 115–121.
68 D. Ding, W. Huang, C. Song, M. Yan, C. Guo and S. Liu, *Chem. Commun.*, 2017, **53**, 6744–6747.
69 G. Ni, N. Miljkovic, H. Ghasemi, X. Huang, S. V. Boriskina, C.-T. Lin, J. Wang, Y. Xu, M. M. Rahman, T. Zhang and G. Chen, *Nano Energy*, 2015, **17**, 290–301.
70 X. Gao, H. Ren, J. Zhou, R. Du, C. Yin, R. Liu, H. Peng, L. Tong, Z. Liu and J. Zhang, *Chem. Mater.*, 2017, **29**, 5777–5781.
71 Y. Wang, L. Zhang and P. Wang, *ACS Sustainable Chem. Eng.*, 2016, **4**, 1223–1230.
72 C. Chen, Y. Li, J. Song, Z. Yang, Y. Kuang, E. Hitz, C. Jia, A. Gong, F. Jiang, J. Y. Zhu, B. Yang, J. Xie and L. Hu, *Adv. Mater.*, 2017, **29**, 1701756.
73 X. Li, R. Lin, G. Ni, N. Xu, X. Hu, B. Zhu, G. Lv, J. Li, S. Zhu and J. Zhu, *Natl. Sci. Rev.*, 2018, **5**, 70–77.
74 L. Shi, Y. Wang, L. Zhang and P. Wang, *J. Mater. Chem. A*, 2017, **5**, 16212–16219.
75 J. Yang, Y. Pang, W. Huang, S. K. Shaw, J. Schiffbauer, M. A. Pillers, X. Mu, S. Luo, T. Zhang, Y. Huang, G. Li, S. Ptasinska, M. Lieberman and T. Luo, *ACS Nano*, 2017, **11**, 5510–5518.
76 Y. Yang, R. Zhao, T. Zhang, K. Zhao, P. Xiao, Y. Ma, P. M. Ajayan, G. Shi and Y. Chen, *ACS Nano*, 2018, **12**, 829–835.
77 A. Guo, X. Ming, Y. Fu, G. Wang and X. Wang, *ACS Appl. Mater. Interfaces*, 2017, **9**, 29958–29964.
78 X. Hu, W. Xu, L. Zhou, Y. Tan, Y. Wang, S. Zhu and J. Zhu, *Adv. Mater.*, 2017, **29**, 1604031.
79 Y. Fu, G. Wang, T. Mei, J. Li, J. Wang and X. Wang, *ACS Sustainable Chem. Eng.*, 2017, **5**, 4665–4671.
80 H. Ren, M. Tang, B. Guan, K. Wang, J. Yang, F. Wang, M. Wang, J. Shan, Z. Chen, D. Wei, H. Peng and Z. Liu, *Adv. Mater.*, 2017, **29**, 1702590.
81 S. M. Sajadi, N. Farokhnia, P. Irajizad, M. Hasnain and H. Ghasemi, *J. Mater. Chem. A*, 2016, **4**, 4700–4705.
82 Z. Liu, H. Song, D. Ji, C. Li, A. Cheney, Y. Liu, N. Zhang, X. Zeng, B. Chen, J. Gao, Y. Li, X. Liu, D. Aga, S. Jiang, Z. Yu and Q. Gan, *Global Challenges*, 2017, **1**, 1600003.
83 W. Xu, X. Hu, S. Zhuang, Y. Wang, X. Li, L. Zhou, S. Zhu and J. Zhu, *Adv. Energy Mater.*, 2018, **8**, 1702884.
84 P. D. Dongare, A. Alabastri, S. Pedersen, K. R. Zodrow, N. J. Hogan, O. Neumann, J. Wu, T. Wang, A. Deshmukh, M. Elimelech, Q. Li, P. Nordlander and N. J. Halas, *Proc. Natl. Acad. Sci. U. S. A.*, 2017, **114**, 6936–6941.
85 S. Zhuang, L. Zhou, W. Xu, N. Xu, X. Hu, X. Li, G. Lv, Q. Zheng, S. Zhu, Z. Wang and J. Zhu, *Adv. Sci.*, 2018, **5**, 1700497.
86 Y. Zeng, K. Wang, J. F. Yao and H. T. Wang, *Chem. Eng. Sci.*, 2014, **116**, 704–709.
87 J. Zhou, Z. Sun, M. Chen, J. Wang, W. Qiao, D. Long and L. Ling, *Adv. Funct. Mater.*, 2016, **26**, 5368–5375.
88 M. W. Higgins, A. R. Shakeel Rahmaan, R. R. Devarapalli, M. V. Shelke and N. Jha, *Sol. Energy*, 2018, **159**, 800–810.
89 F. M. Canbazoglu, B. Fan, A. Kargar, K. Vemuri and P. R. Bandaru, *AIP Adv.*, 2016, **6**, 085218.
90 X. Lin, J. Chen, Z. Yuan, M. Yang, G. Chen, D. Yu, M. Zhang, W. Hong and X. Chen, *J. Mater. Chem. A*, 2018, **6**, 4642–4648.
91 Q. Chen, Z. Pei, Y. Xu, Z. Li, Y. Yang, Y. Wei and Y. Ji, *Chem. Sci.*, 2018, **9**, 623–628.
92 J. Wang, Z. Liu, X. Dong, C.-E. Hsiung, Y. Zhu, L. Liu and Y. Han, *J. Mater. Chem. A*, 2017, **5**, 6860–6865.
93 Q. Jiang, L. Tian, K. K. Liu, S. Tadepalli, R. Raliya, P. Biswas, R. R. Naik and S. Singamaneni, *Adv. Mater.*, 2016, **28**, 9400–9407.
94 Y. Li, T. Gao, Z. Yang, C. Chen, W. Luo, J. Song, E. Hitz, C. Jia, Y. Zhou, B. Liu, B. Yang and L. Hu, *Adv. Mater.*, 2017, **29**, 1700981.
95 Y. Li, T. Gao, Z. Yang, C. Chen, Y. Kuang, J. Song, C. Jia, E. M. Hitz, B. Yang and L. Hu, *Nano Energy*, 2017, **41**, 201–209.
96 Y. Wang, C. Wang, X. Song, S. K. Megarajan and H. Jiang, *J. Mater. Chem. A*, 2018, **6**, 963–971.
97 K.-K. Liu, Q. Jiang, S. Tadepalli, R. Raliya, P. Biswas, R. R. Naik and S. Singamaneni, *ACS Appl. Mater. Interfaces*, 2017, **9**, 7675–7681.
98 X. Wu, G. Y. Chen, W. Zhang, X. Liu and H. Xu, *Adv. Sustainable Syst.*, 2017, **1**, 1700046.
99 N. Xu, X. Hu, W. Xu, X. Li, L. Zhou, S. Zhu and J. Zhu, *Adv. Mater.*, 2017, **29**, 1606762.
100 G. Xue, K. Liu, Q. Chen, P. Yang, J. Li, T. Ding, J. Duan, B. Qi and J. Zhou, *ACS Appl. Mater. Interfaces*, 2017, **9**, 15052–15057.
101 C. Jia, Y. Li, Z. Yang, G. Chen, Y. Yao, F. Jiang, Y. Kuang, G. Pastel, H. Xie, B. Yang, S. Das and L. Hu, *Joule*, 2017, **1**, 588–599.
102 S. Ishii, R. P. Sugavaneshwar, K. Chen, T. D. Dao and T. Nagao, *Opt. Mater. Express*, 2016, **6**, 640–648.
103 S. Ishii, R. P. Sugavaneshwar and T. Nagao, *J. Phys. Chem. C*, 2016, **120**, 2343–2348.
104 M. Kaur, S. Ishii, S. L. Shinde and T. Nagao, *ACS Sustainable Chem. Eng.*, 2017, **5**, 8523–8528.
105 R. Li, L. Zhang, L. Shi and P. Wang, *ACS Nano*, 2017, **11**, 3752–3759.
106 L. Zhang, B. Tang, J. Wu, R. Li and P. Wang, *Adv. Mater.*, 2015, **27**, 4889–4894.
107 X. Huang, Y.-H. Yu, O. de Llergo, S. M. Marquez and Z. Cheng, *RSC Adv.*, 2017, **7**, 9495–9499.
108 G. Ni, S. H. Zandavi, S. M. Javid, S. V. Boriskina, T. A. Cooper and G. Chen, *Energy Environ. Sci.*, 2018, **11**, 1510–1519.
109 M. B. Ross, M. G. Blaber and G. C. Schatz, *Nat. Commun.*, 2014, **5**, 4090.
110 Y. Wang, D. Wan, S. Xie, X. Xia, C. Z. Huang and Y. Xia, *ACS Nano*, 2013, **7**, 4586–4594.
111 X. Xia and Y. Xia, *Front. Phys.*, 2014, **9**, 378–384.
112 Y. Hsiangkuo, G. K. Christopher, H. Hanjun, M. W. Christy, A. G. Gerald and V.-D. Tuan, *Nanotechnology*, 2012, **23**, 075102.

113 L. M. Maestro, P. Haro-González, A. Sánchez-Iglesias, L. M. Liz-Marzán, J. García Solé and D. Jaque, *Langmuir*, 2014, **30**, 1650–1658.

114 L. Zhang, H. Jing, G. Boisvert, J. Z. He and H. Wang, *ACS Nano*, 2012, **6**, 3514–3527.

115 G. Lu, S. Li, Z. Guo, O. K. Farha, B. G. Hauser, X. Qi, Y. Wang, X. Wang, S. Han, X. Liu, J. S. DuChene, H. Zhang, Q. Zhang, X. Chen, J. Ma, S. C. J. Loo, W. D. Wei, Y. Yang, J. T. Hupp and F. Huo, *Nat. Chem.*, 2012, **4**, 310.

116 J. Li and N. Wu, *Catal. Sci. Technol.*, 2015, **5**, 1360–1384.

117 J. M. Luther, P. K. Jain, T. Ewers and A. P. Alivisatos, *Nat. Mater.*, 2011, **10**, 361.

118 A. Comin and L. Manna, *Chem. Soc. Rev.*, 2014, **43**, 3957–3975.

119 B. Li, Q. Wang, R. Zou, X. Liu, K. Xu, W. Li and J. Hu, *Nanoscale*, 2014, **6**, 3274–3282.

120 C. Zhang, C. Yan, Z. Xue, W. Yu, Y. Xie and T. Wang, *Small*, 2016, **12**, 5320–5328.

121 G. Liu, J. Xu and K. Wang, *Nano Energy*, 2017, **41**, 269–284.

122 A. O. Govorov and H. H. Richardson, *Nano Today*, 2007, **2**, 30–38.

123 Z. Qin, Y. Wang, J. Randrianalisoa, V. Raeesi, W. C. W. Chan, W. Lipiński and J. C. Bischof, *Sci. Rep.*, 2016, **6**, 29836.

124 G. Baffou, R. Quidant and C. Girard, *Appl. Phys. Lett.*, 2009, **94**, 153109.

125 M. Gao, C. K. N. Peh, L. Zhu and G. W. Ho, *Adv. Energy Mater.*, DOI: 10.1002/aenm.201800711.

126 X. Li, W. Xu, M. Tang, L. Zhou, B. Zhu, S. Zhu and J. Zhu, *Proc. Natl. Acad. Sci. U. S. A.*, 2016, **113**, 13953–13958.

127 G. Wang, Y. Fu, X. Ma, W. Pi, D. Liu and X. Wang, *Carbon*, 2017, **114**, 117–124.

128 G. Wang, Y. Fu, A. Guo, T. Mei, J. Wang, J. Li and X. Wang, *Chem. Mater.*, 2017, **29**, 5629–5635.

129 Z. Deng, J. Zhou, L. Miao, C. Liu, Y. Peng, L. Sun and S. Tanemura, *J. Mater. Chem. A*, 2017, **5**, 7691–7709.

130 J. Lombard, T. Biben and S. Merabia, *Phys. Rev. Lett.*, 2014, **112**, 105701.

131 O. Neumann, C. Feronti, A. D. Neumann, A. Dong, K. Schell, B. Lu, E. Kim, M. Quinn, S. Thompson, N. Grady, P. Nordlander, M. Oden and N. J. Halas, *Proc. Natl. Acad. Sci. U. S. A.*, 2013, **110**, 11677–11681.

132 M. Elimelech and W. A. Phillip, *Science*, 2011, **333**, 712–717.

133 Z. Liu, Z. Yang, X. Huang, C. Xuan, J. Xie, H. Fu, Q. Wu, J. Zhang, X. Zhou and Y. Liu, *J. Mater. Chem. A*, 2017, **5**, 20044–20052.

134 S. W. L. Ng, G. Yilmaz, W. L. Ong and G. W. Ho, *Appl. Catal., B*, 2018, **220**, 533–541.

135 W. L. Ong, S. W. L. Ng, C. Zhang, M. Hong and G. W. Ho, *J. Mater. Chem. A*, 2016, **4**, 13307–13315.

136 X.-Q. Wang, C. F. Tan, K. H. Chan, K. Xu, M. Hong, S.-W. Kim and G. W. Ho, *ACS Nano*, 2017, **11**, 10568–10574.

137 C. K. N. Peh, M. Gao and G. W. Ho, *J. Mater. Chem. A*, 2015, **3**, 19360–19367.

138 M.-Q. Yang, M. Gao, M. Hong and G. W. Ho, *Adv. Mater.*, 2018, DOI: 10.1002/adma.201802894.

139 C. H. Liow, X. Lu, C. F. Tan, K. H. Chan, K. Zeng, S. Li and G. W. Ho, *Small*, 2018, **14**, 1702268.

140 P. Yang, K. Liu, Q. Chen, J. Li, J. Duan, G. Xue, Z. Xu, W. Xie and J. Zhou, *Energy Environ. Sci.*, 2017, **10**, 1923–1927.

141 L. Kang, D. Tianpeng, L. Jia, C. Qian, X. Guobin, Y. Peihua, X. Ming, W. Z. Lin and Z. Jun, *Adv. Energy Mater.*, 2018, **8**, 1702481.

142 D. Tianpeng, L. Kang, L. Jia, X. Guobin, C. Qian, H. Liang, H. Bin and Z. Jun, *Adv. Funct. Mater.*, 2017, **27**, 1700551.

143 G. Xue, Y. Xu, T. Ding, J. Li, J. Yin, W. Fei, Y. Cao, J. Yu, L. Yuan, L. Gong, J. Chen, S. Deng, J. Zhou and W. Guo, *Nat. Nanotechnol.*, 2017, **12**, 317.